Norwegian University of Science and Technology (NTNU)
Kavli Institute for Systems Neuroscience

The Specificity of Output from Medial Entorhinal Cortex

Master's Thesis
Faculty of Medicine, Department of Neuroscience

Supervisor: Prof. Menno P. Witter

Christin H. Berndtsson
Trondheim, June 2013

ACKNOWLEDGEMENTS

The work presented in this thesis was performed at the Kavli Institute for Systems Neuroscience and Centre for Neuronal Computation (CNC) at the Norwegian University of Science and Technology (NTNU), under the supervision of Professor Menno P. Witter.

Firstly I would like to thank Menno Witter for all his advice and guidance throughout this project. A special thanks to Paulo Giräo for help and assistance and for all the entertaining stories. Thanks also belong to Bruno Monterotti and Grethe Olsen for always being available to answer any of my questions. To all my friends and colleagues in the Witter group, thank you for all the help and support during this project.

I would especially like to thank my good friend and office mate Annelene Dahl for all the fantastic memories and adventures over the years, and for keeping me as close to sane as possible throughout all of this. To the rest of my neuronerds friends, thanks for all the memories! Finally, I would like to thank my friends and family for all their support.

ABSTRACT

The hippocampal formation (HF) and the parahippocampal region (PHR) have been implicated in learning and memory functions. These regions and their subregions form a highly interconnected and complex microcircuitry, where the entorhinal cortex constitutes the nodal point between the hippocampal formation and the cortex. The entorhinal cortex consists of two functionally distinct subregions. It has been suggested that this difference in functional output results from differences in microcircuitry, and input and output characteristics within the regions. Therefore, in order to understand the function of the entorhinal cortex and how it contributes to the rest of the HF-PHR network, it is necessary to understand the microcircuitry within the region.

This study investigates the specificity of output from cell populations located in superficial layers of the medial entorhinal cortex. Fluorescent retrograde traces were injected into dorsal dentate gyrus (DG) and the dorsal medial entorhinal cortex (MEC). Additional immunohistochemistry was performed in order to investigate the chemical markers for the retrogradely labelled cell populations. Labelled cells and possible colocalization of markers were analysed with fluorescent microscopy. The results indicate the presence of at least three separate cell populations in superficial layers of MEC with different projection patterns and chemical markers. It remains to be seen how the cell populations described here relate to the functionally defined cell populations found in MEC.

TABLE OF CONTENTS

ABBREVIATIONS

General:

HF – Hippocampal formation

PHR – Parahippocampal region

DG – Dentate gyrus

CA – Cornu Ammonis

Sub – Subiculum

PrS – Presubiculum

PaS – Parasubiculum

EC – Entorhinal cortex

MEC – Medial entorhinal cortex

LEC – Lateral entorhinal cortex

PER – Perirhinal cortex

POR – Postrhinal cortex

DHPC – Dorsal hippocampal commissure

VHPC – Ventral hippocampal commissure

CB1R – Cannabinoid type 1 receptor

CCKBC's - cholecystokinin and cannabinoid type 1 receptor (CB1R) expressing basket cell

DSI – Depolarization-induced suppression of inhibition

GAD67 – Glutamate decarboxylase 67

Tracers and solutions:

CB – Calbindin

CR – Calretinin

PV – Parvalbumin

eGFP –enhanced Green fluorescent protein

FB – Fastblue

FG – Fluoro-Gold

DMSO - Dimethyl sulfoxide

PB – Phosphate buffer

PBT – Phosphate buffer Triton-X

1. INTRODUCTION

The hippocampal formation is one of the most studied structures in the brain and has captivated neuroscientists ever since Cajal described its anatomy in 1881 (Bentivoglio & Swanson, 2001). The anatomical organization of the hippocampal formation (HF) and the adjacent parahippocampal region (PHR) have been preserved across phylogeny allowing scientists to utilize animal models to infer knowledge about its function in humans (Amaral & Lavenex, 2007). The hippocampal formation and parahippocampal region have been implicated in memory and learning (Scoville & Milner, 1957), and more recently in several aspects of spatial navigation (Hafting et al., 2005, O´Keefe & Dostrovsky, 1971, Solstad et al., 2008).

Over 60 years ago, in 1948, Edward Tolman suggested that animals form a cognitive map of their spatial environment upon learning (Tolman, 1948). With the discovery of place cells in the hippocampus in 1971, it was hypothesized that these cells produced the cognitive map suggested by Tolman two decades earlier (O´Keefe & Dostrovsky, 1971, O´Keefe, 1976). Place cells fire when the animal is in specific locations within the environment and have been associated with hippocampal pyramidal cells (O´Keefe, 1976). Other spatially modulated cells have later been found in other areas of the hippocampal – parahippocampal system, including, head direction cells, grid cells, border cells and conjunctive cells (Fyhn et al., 2004, Solstad et al., 2008, Taube, 1998, Sargolini et al., 2006).

Grid cells are characterized by multiple firing locations, collectively forming a hexagonal pattern covering the entire environment of the animal (Hafting et al., 2005). Studies have shown that the spatial scale of grid cells increase progressively in a step-like manner from dorsal to ventral in MEC (Brun et al., 2008b, Stensola et al., 2012). Spatially modulated cells like place and grid cells have been found in several phylogenically distant species (Yartsev et al., 2011, Killian et al., 2012). Thus, insights into the connectivity and functionality of these cell types and the regions contributing to the HF-PHR system are believed to be transferable to humans (Ekstrom et al., 2003, Doeller et al., 2010).

The HF-PHR system is made up of highly interconnected subregions with a complex microcircuitry. Multimodal information from the cortical mantle converges onto the parahippocampal region which subsequently processes and relays this information to the hippocampal formation. After passing through the hippocampal circuit, the information is relayed back to the cortical mantle through the parahippocampal region (Van Strien et al., 2009). The insights into the anatomy, connectivity and function of the hippocampal formation are more detailed than that of its adjacent input-output region,

the entorhinal cortex (Canto et al., 2008). This region can be subdivided into two anatomically similar but functionally different regions (Eichenbaum et al., 2007). It has been hypothesized that this difference in function is generated by differences in intrinsic wiring in combination with highly specific inputs (Canto et al., 2008). In order to fully understand the functionality of this complex and interconnected system it is therefore vital to understand the microcircuitry and intrinsic wiring of each sub region.

1.1. Anatomy of the hippocampal and parahippocampal region

1.1.1. Nomenclature

The hippocampal formation and parahippocampal region have been extensively studied over the last century. In spite of this rigorous study, there are still substantial disagreement with regards to the terminology of the various regions, and even which regions should be included under each term (Witter & Amaral, 2004).

In this thesis I have chosen to adopt the nomenclature put forth by Insausti et al (1997), where the Hippocampal Formation (HF) is comprised of the dentate gyrus (DG), the three subfields of Cornu Ammonis (CA), CA1, CA2 and CA3, and the subiculum (Sub). These structures all share a tree-layers appearance and are therefore classified as allocortex. The adjacent parahippocampal region (PHR) consists of the presubiculum (PrS), the parasubiculum (PaS), the entorhinal cortex (EC), and the perirhinal (PER) and postrhinal (POR) cortices.

1.1.2. Axes of the hippocampal formation and the parahippocampal region

In the rat, the hippocampal formation is situated in the caudal part of the brain. It extends in a C-shaped manner from a medial and rostrodorsal position directly dorsal to the septal nuclei of the basal forebrain to a more caudoventral position adjacent to the amygdala. The parahippocampal region wraps around the more caudal and ventral portions of the hippocampal formation (Figure 1).

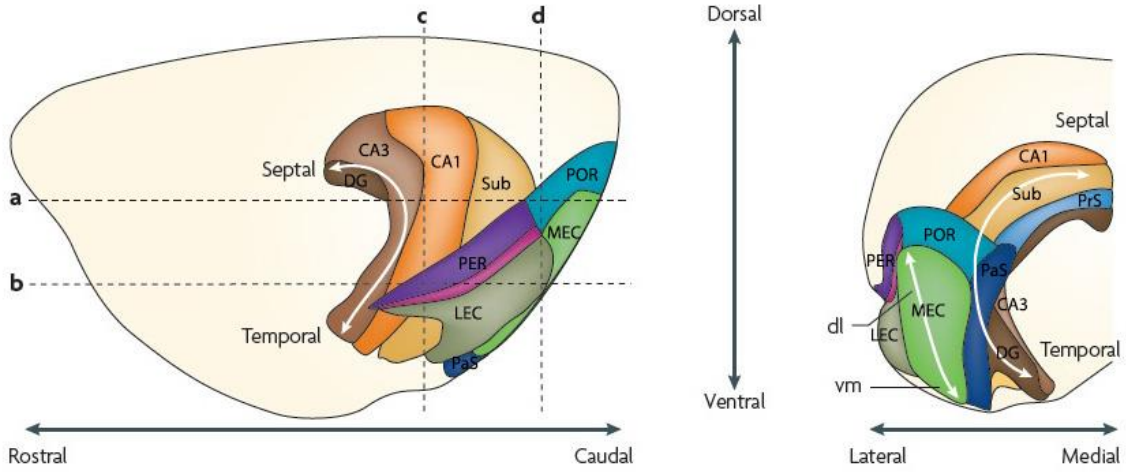

Figure 1: The position of the HF and PHR in relation to the septotemporal, dorsoventral, and medial-lateral axes. Regions included: The hippocampal formation in brown and orange shades including, dentate gyrus (DG), subfields of Cornu Ammonis, CA1 and CA3, and Subiculum (Sub). The Parahippocampal region in green, blue and purple shades, Presubiculum (PrS), Parasubiculum (PaS), Medial Entorhinal cortex (MEC), Lateral Entorhinal cortex (LEC), Perirhinal cortex (PER) and Postrhinal cortex (POR). Figure adapted from (Van Strien et al., 2009).

The long axis of the hippocampal formation is referred to as the septotemporal axis (Figure 1), while the orthogonal axis is referred to as the transverse or proximal-distal axis. For the latter axis proximal refers to the part of the region closest to the dentate gyrus, while distal refers to the part closest to the entorhinal cortex. The radial (deep–superficial) axis refers to the position within the lamina (Figure 2).

The parahippocampal region is not described along a septotemporal axis, but rather along a dorsoventral axis (Figure 1). Positions along the transverse axis within the parahippocampal region are generally not referred to as proximal or distal, but as the mediolateral axis. Here, a lateral position indicates a position close to the rhinal fissure, while a more medial position indicates closer to the border between the parahippocampal region and the hippocampal formation. Additionally, there is a radial or deep to superficial axis when discussing the position within a specific layer (Figure 2) (Amaral & Lavenex, 2007).

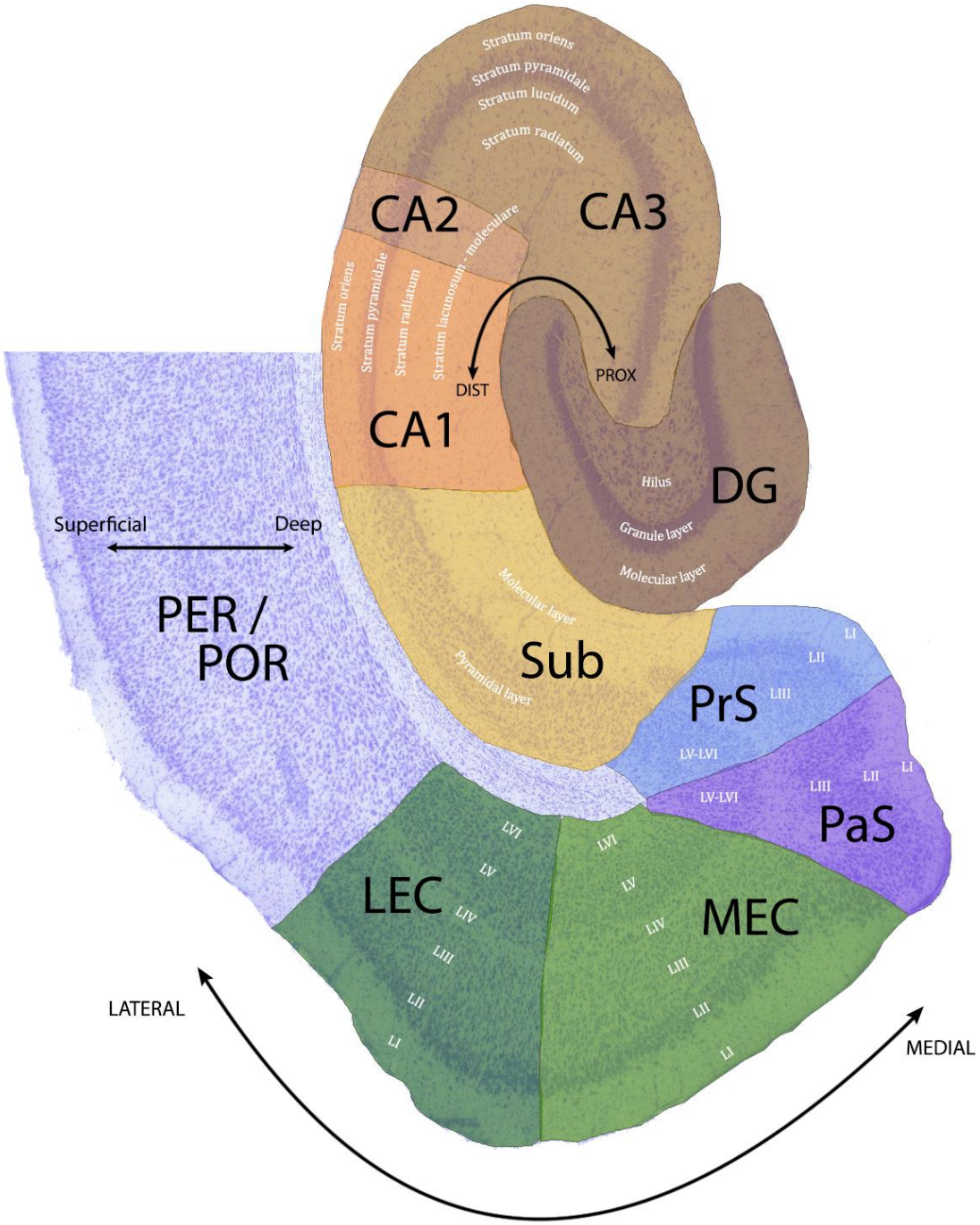

Figure 2: Horizontal section of the rat hippocampal and parahippocampal region overlaid with a counterstained Cresyl violet section to visualize cells bodies. Indicated are the proximal-distal and medial-lateral axes of HF and PHR. Regions are colour-coded with the hippocampal formation in brown and yellow tones, including Dentate gyrus (DG), subfields of Cornu Ammonis, CA3, CA2, and CA1, Subiculum (sub), and the parahippocampal region in blue and green tones, including Presubiculum (PrS), Parasubiculum (PaS), Medial entorhinal cortex (MEC), and Lateral entorhinal cortex (LEC). Layers in each sub region are labelled in white.

1.2. Architecture of the hippocampal formation

The hippocampal formation can, as described above, be subdivided into 5 cytoarchitectonically different regions (Figure 2). These regions all have an archicortical three-layered appearance, where the principal cell layer lies in between a superficial and a deep polymorph or cell sparse layer.

1.2.1. Dentate gyrus

The principal cell type of the dentate gyrus is the granule cell. These cells sit close together in the granule cell layer. They extend spiny dendrites toward the superficial portion of the molecular layer, where the perforant path input from entorhinal cortex and inputs from the contra-and ipsilateral dentate gyrus terminate. The granule cells give rise to the mossy fibre projection which terminates in the neighbouring CA3 region. The deep layer of the dentate is often referred to as the hilus, in which mossy cells give rise to the associational and commissural projections terminating in the inner third of the molecular layer (Amaral & Lavenex, 2007). The DG is often described in relation to its two blades. The enclosed blade, often referred to as the inner blade lies adjacent to the CA1, while the exposed blade, often referred to as the outer/free blade lies opposite the enclosed blade (Kjoningsen et al., 2011).

1.2.2. The subfields of Cornu Ammonis

The CA fields all share a similar layered organization, and will therefore be discussed together. The principal cell layer of all subfields is the pyramidal cell layer (Figure 2), and is as the name suggests, mostly made up of pyramidal neurons. Deep to the pyramidal cell layer lays the stratum oriens containing the basal dendrites of pyramidal neurons. Superficial to the pyramidal cell layer in CA1 and CA2 lays the stratum radiatum. In CA3 the stratum radiatum is separated from the pyramidal cell layer by a thin acellular layer called stratum lucidum, in which the mossy fibre projection from the dentate gyrus terminates. The CA3-CA3 associational projections and the CA3-CA1 Shaffer collateral projections both terminate predominantly in stratum radiatum. The most superficial layer of the hippocampus is called the stratum lacunosum-moleculare, were the fibres from entorhinal cortex and other regions terminate (Amaral & Lavenex, 2007).

1.2.3. Subiculum

The principal cell layer of the subiculum is the pyramidal cell layer. Compared to that in the adjacent CA1, the subicular pyramidal cell layer is much wider, including multiple layers of neurons (Figure 2). Superficial to this lies the molecular layer, which can be further subdivided into a deep and a superficial part, where the deep part is continuous with the stratum radiatum of CA1 and the superficial part with

the stratum lacunosum-moleculare. The projection from CA1 to subiculum terminates in the deep part of the molecular layer, and adheres to a strict topography, where cells located proximally in CA1 project distally in the subiculum, and cells located in distal CA1 project across the border to proximal subiculum. The superficial portion of the molecular layer receives projections from the entorhinal cortex. The subiculum gives rise to projections to the entorhinal cortex, pre-and parasubiculum and other cortical areas, and is therefore generally considered as the main output region of the hippocampal formation (Amaral & Lavenex, 2007).

1.3. Architecture of the parahippocampal region

The parahippocampal region has been subdivided into 5 separate regions (Figure 2). Although there have been some controversy whether pre-and parasubiculum should be considered as having 3 or 6 layers, these structures are generally considered to be six layered (Witter & Amaral, 2004).

1.3.1. Presubiculum and parasubiculum

The presubiculum can be easily distinguished from the subiculum by its densely packed superficial layers of small pyramidal neurons. Deep to the superficial layers is a cell free zone separating the superficial from the deep layers. This cell free zone is continuous with the lamina dissecans of entorhinal cortex. The deeper layers of presubiculum appear to be continuous with the deep layers of parasubiculum and the principal cell layer of subiculum. The parasubiculum can be distinguished from the presubiculum on the basis of cells in the superficial layers. In contrast with presubiculum, layer II and III of parasubiculum consists of large, densely packed pyramidal neurons. The deeper layers of parasubiculum are considered to be continuous with those of the entorhinal cortex, comparable to what is seen in case of the presubiculum (Witter & Amaral, 2004).

1.3.2. Entorhinal cortex

The entorhinal cortex lies directly adjacent to the parasubiculum, in the rostrocaudal part of the cerebral hemisphere of the rat. Several nomenclatures have been proposed with regards to the laminar subdivision of the region. In this thesis I have adopted the nomenclature put forth by Santiago Ramón y Cajal in 1911. Here the entorhinal cortex is subdivided into six distinct layers, with four cellular layers (layers II, III, V, and VI) and two acellular layers (layer I, and layer IV or lamina dissecans). The entorhinal cortex plays a very important role in information flow to and from the hippocampal formation as it holds a nodal position in the hippocampal–cortical circuits (Amaral & Lavenex, 2007). The organization of the entorhinal cortex and its connectivity will be discussed in greater detail below.

1.3.3. Perirhinal and postrhinal cortices

The perirhinal and postrhinal cortices makes up the last regions of the parahippocampal formation. Both were previously considered to be perirhinal cortex, but a further differentiation was proposed based on cytoarchitecture and connectivity in the rat (Burwell et al., 1995, Burwell, 2001). The regions can be characterized as agranular and/or dysgranular cortex, with a relatively homogeneous transition between layers III and V. The characteristic lamina dissecans from the neighbouring entorhinal cortex is not present. The peri- and postrhinal cortices receive inputs from different cortical regions, and project differently onto the entorhinal cortex, with perirhinal cortex projecting mainly to lateral entorhinal cortex, and postrhinal mainly targeting the medial entorhinal cortex (Amaral & Lavenex, 2007).

1.4. The entorhinal cortex

The entorhinal cortex (EC) can be subdivided into two cytoarchitectonically and functionally distinct subregions, the medial (MEC) and lateral (LEC) entorhinal cortex (Insausti et al., 1997, Kerr et al., 2007). LEC occupies the rostrolateral portion of EC with borders to perirhinal cortex, while MEC lies medial and caudal to LEC bordering the parasubiculum. Several cytoarchitectonic characteristics can be used to separate the two regions. Cells in LII of LEC are densely packed and clustered into islands, while cells in the same layer of MEC are generally larger in size, and do not show this characteristic clustering. The lamina dissecans is sharply delineated in MEC, while less clear in LEC, and deeper layers of MEC show a columnar arrangement which is not obvious in its lateral counterpart. The border between LEC and perirhinal cortex can easily be established as the lamina dissecans disappears, and the lamination becomes more homogenous. The border between MEC and parasubiculum can be distinguished by a striking merge of LII and LIII in parasubiculum compared to the easily separated LII and LIII in MEC (Witter & Amaral, 2004, Kjoningsen et al., 2011). The borders between MEC and LEC, and the adjacent regions can be seen in figure 2.

Due to its nodal position between the hippocampal formation and the rest of the cortex, the EC can greatly influence the flow of information to and from the hippocampal formation. MEC and LEC receive inputs from different sources, with the main input to MEC coming from the postrhinal cortex, while the LEC receives its main inputs from the perirhinal cortices. In turn both MEC and LEC contribute to the perforant path projection to HF (Witter & Amaral, 2004). As this thesis is primarily concerned with the medial entorhinal cortex, I will focus on the cell types and connectivity of this region in the sections below.

1.4.1. The medial entorhinal cortex

Layer I

Layer I (LI) of MEC has a rather homogeneous appearance, and is densely packed with fibres from, among others, the presubiculum and postrhinal cortex (Witter & Wouterlood, 2002). Neurons in LI are generally considered to be GABAergic, and are scattered throughout the layer, with cell bodies mainly located in deep LI. The majority of LI neurons are classified as multipolar neurons, while the remaining cells are considered to be horizontal cells. Both cell types have apical dendrites radiating within LI and basal dendrites extending into LII (Canto & Witter, 2011).

Layer II

Layer II (LII) consists of two main types of neurons, the stellate cell (SCs), preferentially located in the superficial and middle third of LII, and the pyramidal cell, mainly located in the deep one third of LII. Klink and Alonso (1997) reported that 65% of cells with stellate-like electrophysiological properties proved to have stellate morphology after reconstruction of the cell. They further reported that cells that did not show this characteristic stellate like electrophysiology were found to be either pyramidal-like (32%) or horizontal-like in morphology (3%). It is generally assumed that stellate cells are grid cells (Couey et al., 2013), although Domnisouru et al (2013) reported grid cells with pyramidal morphology. Furthermore, grid cells can be found in layers without stellate cells, indicating that other cell types can generate grid properties (Sargolini et al., 2006).

Stellate cells have been shown to have an elongated ovoid somata, with between two and 11 primary dendrites arising from the soma. The main axon of the SCs travels towards the angular bundle, and has been found to either arise directly from the soma, or from a primary dendrite close to the soma. Pyramidal neurons have ovoid or pyramidal shaped somata with one prominent thick apical dendrite arising from the soma, and several thin and short basal dendrites radiating from all around the soma. The main axon leaves the soma and travels toward the angular bundle (Canto & Witter, 2011, Klink & Alonso, 1997). Figure 3 shows camera lucida drawings of typical stellate and pyramidal neurons.

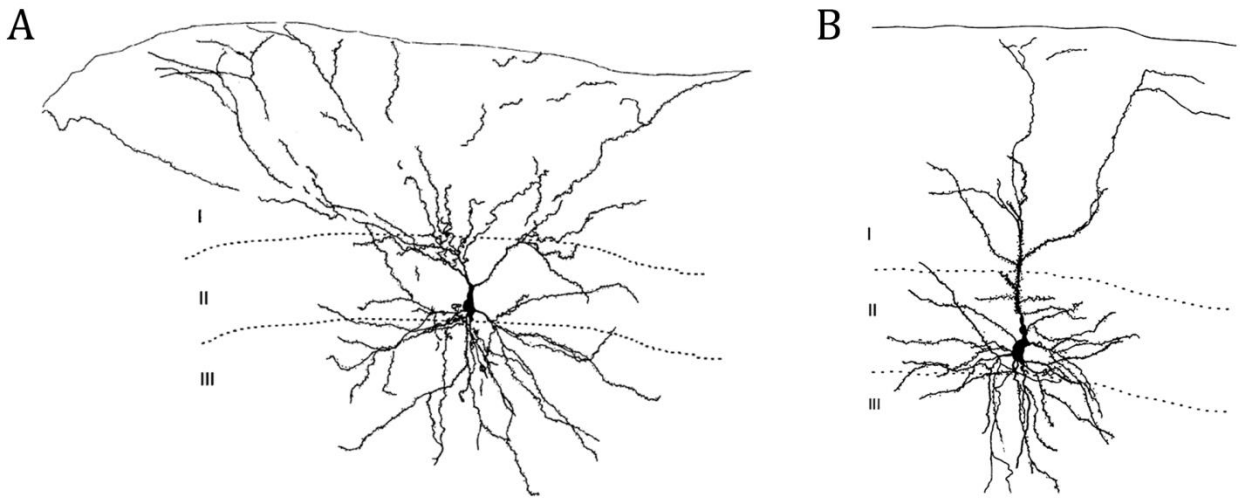

Figure 3: Morphology of a typical stellate cell (A), and a typical pyramidal cell (B). Modified from Klink and Alonso (1997).

The subdivision of cell types in LII into SCs and pyramidal cells has been further elaborated by Canto et al (2011) to include a total of five cell types. In addition to the already described stellate and pyramidal cell, they report the existence of three intermediate pyramidal neurons. The oblique pyramidal neurons have a horizontally oriented soma, one main apical dendrite extending towards the pia, and thin, short basal dendrites. The last two types both have pyramidal shaped somatas, one with the apex facing the pia, which is similar to the pyramidal neuron, and one with a horizontally oriented soma, similar to the oblique pyramidal neuron. Both cell types have multiple apical dendrites, placing the morphology in between that of a typical stellate, pyramidal and oblique pyramidal neuron. These three intermediate cell types either have a SC physiology or a pyramidal physiology, with 50% of the oblique pyramidal cells and 73% of the two last intermediate cell types showing membrane oscillations characteristic of SCs (Canto & Witter, 2011).

Layer III

Five cell types, including stellate cells, multipolar cells, and three types of pyramidal neurons populate layer III (LIII). The small spiny pyramidal neuron is located throughout LIII, has one apical dendrite and basal dendrites radiating from the cell body in different directions. The complex pyramidal neuron preferentially resides in the middle to deep third of LIII, and can in contrast to small pyramidal neurons have two apical dendrites. Its basal dendrites radiate in many directions, but are generally confined to LIII. The bipolar complex pyramidal neurons have one or two apical dendrites, a round to pyramidal shaped soma and one prominent basal dendrite branching horizontally within LIII. The multipolar neurons also reside in the middle to deep third of LIII, but are preferentially located close to the border with parasubiculum. Lastly, the stellate cells in LIII are located superficially within the layer, they have

one frequently splitting apical dendrite, and basal dendrites which reside within superficial LIII (Canto & Witter, 2011).

Layer IV

Layer IV (LIV), also referred to as the lamina dissecans is a thin fibre rich layer, separating the deep and superficial layers of EC. Though many consider this a cell free layer, scattered cells in LIV have been reported like fusiform and pyramidal cells (Lingenhöhl & Finch, 1991). LIV neurons can generally be said to show similar physiology and morphology as either LIII or LV neurons (Canto & Witter, 2011).

Layer V and VI

Layer V (LV) neurons have been subdivided into three main classes of neurons, mainly pyramidal, horizontal and polymorph cells (Hamam et al., 2000). This classification was further elaborated by Canto et al (2011) who proposed to classify LV neurons into three types of pyramidal neurons, superficial and deep pyramidal neurons, where the superficial cell type has larger somata compared to the deep pyramidal cells, and lastly a bipolar pyramidal neuron group. A fourth group comprises of a continuum of cells from tilted pyramidal cells to multipolar cells. Layer VI (LVI) pyramidal neurons can be subdivided into fewer classes compared to LV. Here pyramidal neurons have been subdivided into either a horizontal pyramidal neuron with dendrites travelling parallel to the layer or a tilted pyramidal neuron with dendrites facing the subiculum. The last group of neurons in LVI consists of multipolar neurons with similar length dendrites extending from the soma in all directions (Canto & Witter, 2011).

1.4.2. Connectivity of the medial entorhinal cortex

Interconnectivity between layers

The different layers of MEC have intralaminar connections, with cells in each layer projecting both in mediolateral and dorsoventral directions within the layer. In both LII and LIII the dorsoventral projection runs largely in the ventral direction within the layer. Layer V show projections to all superficial layers of MEC (Köhler, 1986). Layers II-III both project to deeper layers, though evidence suggests that they do not terminate here, but rather passes through on their way to other regions. Nonetheless, it has been suggested that these layers may still form synapses with cells in LV and LVI while passing through (Köhler, 1986). In contrast to the superficial to deep projection, van Haeften et al (2003) showed that deeper layers of EC project to superficial layers of EC, branching within LIII, superficially in LII and deep in LI. This projection provides a feedback loop from the HF to the superficial layers of EC (Kloosterman et al., 2003).

Extrinsic connections

The entorhinal cortex projects to the different subregions of the hippocampal formation through the fibre pathway called the perforant path. This projection can be subdivided into two components termed the medial and the lateral perforant pathway, based on their origins in MEC or LEC respectively. These two pathways have further been subdivided into a LII and a LIII component with different targets in the hippocampal formation. The LII component sends projections to DG and CA3, while the LIII component project mainly to CA1 and subiculum (Witter, 2007). The organization of the LII component to DG will be discussed in greater detail below.

Entorhinal-dentate projection

Both the ipsilateral and the contralateral projection from EC to DG arise mainly from cells located in LII. A minor projection also arises from deeper layers. These projections can be described along the three axes of DG, the radial, transverse and the longitudinal axis (Witter, 2007, Steward & Scoville, 1976).

The radial axis extends through the layers of DG, from deep to superficial. Fibres of the medial perforant path terminate on parts of dendrites located in the middle one-third of the molecular layer, while the lateral perforant path terminates on parts of dendrites located in the outer one-third. The projection from deeper layers of EC terminates mainly in the inner one-third of the molecular layer, the granule layer and in the hilus. It is generally believed that the input from both the medial and the lateral pathway converges onto one single granule cell, although conclusive anatomical evidence for this has yet to be found (Witter, 2007).

The transverse axis lies perpendicular to the dorso-ventral, or longitudinal axis of DG. There is some conflict with regard to the transverse termination pattern of perforant path fibres. Wyss (1981) found that the lateral perforant path mainly target the enclosed blade of DG, while the medial perforant path projections either does not have a preference for the exposed or the enclosed blade, or mainly project to the exposed blade. However, Witter (2007) reported little difference in the organization of termination patterns from the medial and lateral perforant path. The lateral perforant path did however show some preference for the enclosed blade, as labelling was denser in this blade compared to the exposed blade.

The entorhino-dentate projection shows a remarkable organization along the longitudinal axis of DG. Cells located dorsolaterally within EC project to the dorsal part of DG, while projections from the more ventromedial EC terminate in more ventral levels of DG. This organizational pattern results in

projections from lateral LEC and lateral and caudal parts of MEC targeting dorsal parts of DG, while the more medial parts of both LEC and MEC project to ventral portions of DG (Witter, 2007). This topographical organization was beautifully illustrated by Dolorfo and Amaral (1998) by injecting retrograde tracers at different dorsoventral levels of DG. These injections resulted in almost non overlapping populations of labelled cells from lateral to more medial positions in EC based on the dorso-ventral level of the injection site. Furthermore EC cells have been shown to originate highly collateralized axons innervating several levels of DG (Witter & Amaral, 1989).

Commissural projections

The entorhinal cortex has relatively strong commissural projections to both the contralateral entorhinal cortex and other regions of the contralateral hippocampal formation. These projections arise from all portions of EC (Amaral & Lavenex, 2007). Entorhinal commissural projections have been studied in several species, and appear to arise mainly from LIII of EC (Steward & Scoville, 1976). However, Köhler (1978) reported that commissural projection originated both in LII and LIII of the rat EC. In other species, commissural projections have been reported to arise from LIII of the monkey, and both LII and LIII in the cat (Ino et al., 2000, Amaral et al., 1984). The commissural projection between EC regions can be described as a very focal projection, meaning that a small part of EC will project to a similarly small homotopic part of the contralateral EC (Amaral & Lavenex, 2007). Adelmann et al (1996) investigated the fibre tracts in the fimbria fornix complex of the rat, and showed a clear separation of the different commissural projections. The entorhino-entorhinal commissural projections pass exclusively through the dorsal hippocampal commissure (DHPC), while commissural projections between EC and HF regions pass through the ventral hippocampal commissure (VHPC).

1.4.3. Immunoreactivity of the medial entorhinal cortex

Several populations of neurons can be detected in the entorhinal cortex based on immunoreactivity to different proteins and neuropeptides. These markers are often inhomogeneously distributed along the dorsoventral, medial- lateral and the radial axes of EC. Additionally, these markers often colocalize with each other, and/or with GABA or its synthesising enzyme GAD (Witter & Wouterlood, 2002). For instance the calcium- binding proteins Calbindin (CB), Calretinin (CR) and Parvalbumin (PV) are all differently distributed throughout EC. All three markers are expressed in several types of interneurons, but in contrast to CR and PV, Calbindin has also been shown to be expressed in cells contributing to the perforant path projection (Witter & Wouterlood, 2002). All three markers are also to different degrees colocalized with GABA. While all PV neurons have been reported to express GABA, opinions differ with relation to CR neurons, where reports range from 30-100% colocalization (Miettinen et al., 1997,

Wouterlood et al., 2000, Miettinen et al., 1996). Some CB neurons are also reported to colocalize with GABA, most abundantly in LII-LIII of LEC (Witter & Wouterlood, 2002, Wouterlood & Jasperse, 2001).

In addition to the three calcium binding proteins mentioned above, cells in EC have been reported to express several neuropeptides like somatostatin, and cholecystokinin (Witter & Wouterlood, 2002, Wouterlood & Pothuizen, 2000).

1.5. Separating cell populations in EC

Varga et al (2010) found that cell populations in MEC LII can be separated based on their immunoreactivity to reelin and calbindin. They report that cells projecting to DG, making up parts of the perforant path projection are positive for reelin, but negative for calbindin. Additionally, cells projecting to the contralateral MEC are reported to be positive for calbindin while negative for reelin. Adding to this microcircuitry, Varga et al (2010) showed that the cholecystokinin and cannabinoid type 1 receptor (CB1R) expressing basket cell (CCKBC's) only formed synaptic contacts with the calbindin positive cell population (Figure 4). Electrophysiology and *post hoc* immunohistochemistry was used to further test this specificity. As the CCKBC's express CB1R they exhibit a short-term plasticity mechanism known as depolarization-induced suppression of inhibition (DSI) (Diana & Marty, 2004). Calbindin positive cells were found to exhibit DSI, while most reelin neurons did not (Varga et al., 2010).

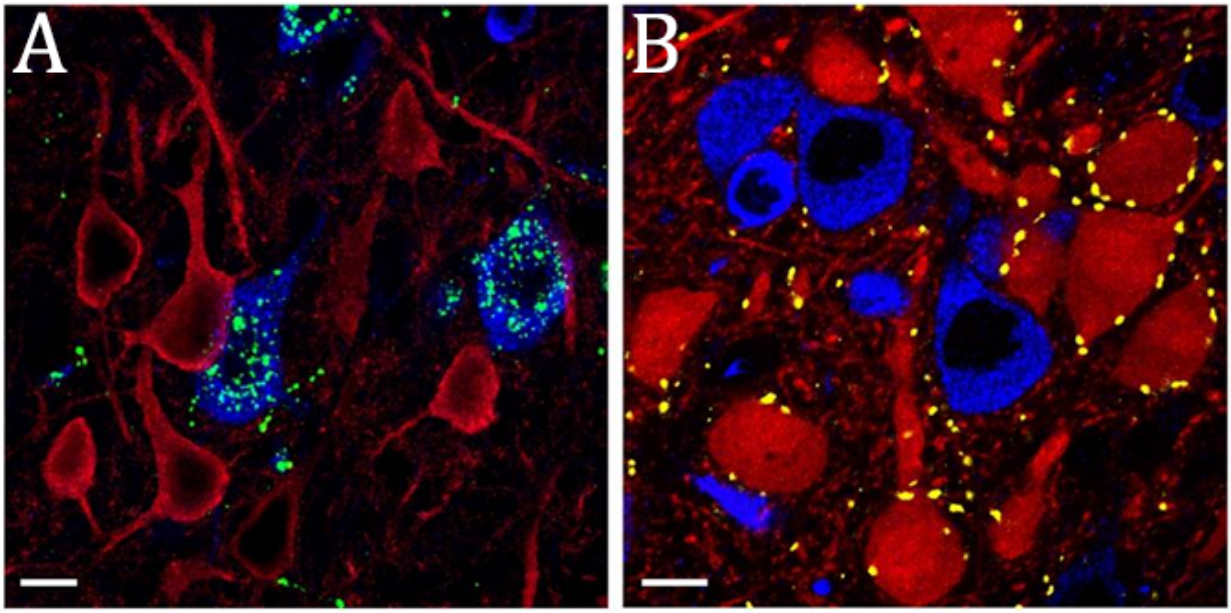

Figure 4: Reelin and calbindin positive cells in LII of MEC. *Red:* Calbindin. *Blue:* Reelin. A: Retrogradely transported BDA from ipsilateral DG label only reelin positive cells. BDA visualized in green. B: Terminals of CCKBC's surround calbindin immunoreactive cells while avoiding reelin positive cells. Terminals of CCKBC's are visualized in yellow. Adapted from Varga et al (2010).

Based on these results it can be possible to use the markers reelin and calbindin to separate the commissurally projecting cell population and the perforant path projecting population in MEC. Furthermore, the GABAergic microcircuit specialization exhibited by CCKBC's allows these cells to selectively innervate information processing. Both the cellular markers and this selective GABAergic innervation can have unknown implications on the functionally defined cell populations in MEC, mainly grid and border and head direction cells (Krook-Magnuson et al., 2012).

These results are however in conflict with previously reported data concerning commissural projections in MEC. While Varga et al (2010) claim that cell populations within MEC LII can be separated into an entorhinal–dentate projecting and an commissural projecting population, previous studies on the commissural projection reports that it arise mainly from LIII of EC (Köhler et al., 1978, Steward & Scoville, 1976).

1.6. Aim

The results presented by Varga et al (2010) highlight the importance of investigating and understanding the anatomical wiring of a network in order to gain insights into the possible functions of the system. The hippocampal formation and parahippocampal region form a highly interconnected and functionally complex system, where each subregion is uniquely wired and contributes to different functions within a larger system. As mentioned earlier, several functionally defined cell populations have been found in these regions, including the grid cells.

Superficial layers of MEC are known to have several anatomically different types of principal cells and specific projection targets. Understanding the wiring of these cell populations and their projection patterns are important in order to understand the information flow within the system. As the results presented by Varga et al (2010) are in conflict with previously reported projection patterns within MEC, it is necessary to investigate this connectivity further.

The aim of this project is therefore to study the specificity of output from projection cells in superficial layers of MEC. I will furthermore try to replicate the findings presented by Varga et al (2010) in as much detail as possible.

2. METHODS

2.1 Animals

A total of 36 female Sprague Dawley rats and three in-house bred GAD67-eGFP positive mice were used for this study. The female Sprague Dawley rats were ordered from Charles River, Germany. To ensure animal welfare, all animals had free access to food and water and were kept in rooms with a 12 hour light cycle. All animals were housed and treated according to regulations provided by Forsøksdyrutvalget (The Norwegian Research Authority). The protocols regarding surgery, tissue collection and immunohistochemistry described here were used for both rat and mice experiments unless otherwise is specified.

2.2 Surgery

2.2.1. Anaesthesia and analgesia

Animals were anesthetized using an induction chamber filled with oxygen containing 4% isoflurane, flowing at 1L per minute. Isoflurane was subsequently used as the general anaesthesia and administered through a mouthpiece. The isoflurane level was lowered throughout the surgery, starting at 3% and gradually adjusted to 1%.

Approximately 30 minutes prior to surgery animals were injected subcutaneously with the analgesic Temgesic (0.3mg/mL) and Atropine (0.04mg/kg). Additionally the local anaesthetic Marcain (2.5mg/mL) was injected subcutaneously along the scull of the animal prior to incision. Sterile saline was administered to the animal throughout the surgery to keep the animal hydrated. After surgery, the analgesic Metacam (0.5mg/mL) was administered orally. The effect of Metacam lasts for 8-12 hours, and was therefore given to the animals in the days following surgery to ensure that they did not experience any pain from the procedure.

2.2.2. Surgical procedure

Prior to surgery, animals were weighed and the surgical area shaved. Subsequently, the animal was placed in an induction chamber containing Isoflurane at a concentration of 4% with a flow of 1L per minute. After ensuring that the animal was fully anesthetized by checking toe pinching and eye reflexes, the animal was placed in a stereotaxic frame (Kopf, Tujunga, USA). Earbars were used to fix the position of the animal's head in the frame. After injection of Marcain, the head was disinfected with iodine and alcohol. An incision was made along the midline of the skull and the periost was scraped to the sides

using the scalpel and cotton swabs. Height measurements of lambda and bregma (Figure 5) were used as reference points to ensure that the skull was level. A hole was drilled through the scull at the midline to reveal the sagittal sinus, which together with bregma and lambda served as reference points to calculate further coordinates.

Retrograde tracers were injected (150-250nL) in the dorsal dentate gyrus of the hippocampus in one hemisphere and the MEC in the other hemisphere with a 1µL Hamilton syringe (Hamiltoncompany, USA). The syringe was kept in place for 15 minutes after injection to ensure that the tracer had time to diffuse, before it was slowly removed from the brain.

Once the injection was completed and the syringe removed from the brain, the skin and scull were cleaned with saline solution and the skin was sutured. Iodine was again applied to the skin to disinfect the area and the rat was placed in a heating chamber to recover. When the animal was awake and had regained normal functions, Metacam was administered orally as an analgesic. The animal was then returned to the home cage, and monitored in the days post surgery. A detailed surgery protocol, including coordinates, equipment and tracers can be found in Appendix II.

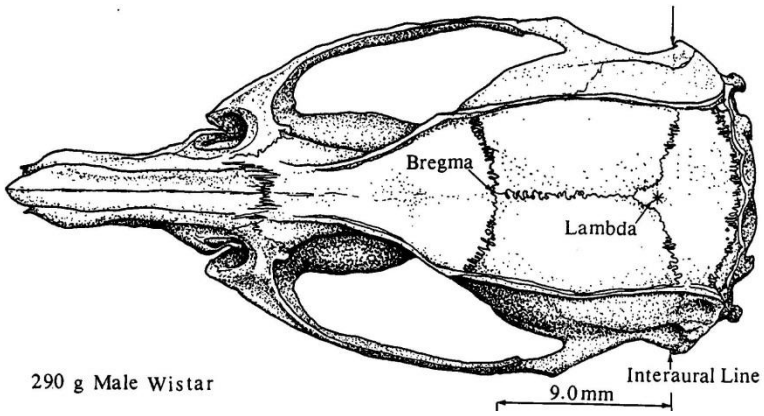

Figure 5: Position of Bregma and Lambda on the dorsal surface of the scull of a rat. Illustration has been adapted from (Paxinos & Watson, 2007).

2.3 Tracers

Neuroanatomical tract-tracing has since its discovery in 1971 (Kristensson & Olsson, 1971) become the fundamental method of revealing the anatomical wiring of the nervous system. Macromolecules can be taken up anywhere along the outer membrane of a neuron and be transported by way of diffusion or active transport in vesicles. Anatomical tract-tracing techniques take advantage of this mechanism by depositing a tracer at a specific stereotactic coordinate to label neurons in this region. Tracers can be

categorized as retrograde or anterograde, depending on the direction of transport relative to the cell body. Retrograde tracers are taken up by the axon terminals and transported back to the soma, while anterograde tracers are taken up by the cell body or dendrites and transported to the axon terminals. The mechanism of uptake, transport and labelling of the cell varies between tracers. (Lanciego & Wouterlood, 2011). For the present study, we used only fluorescent retrograde tracers, which are directly visible in a fluorescence microscope without further processing of the tissue. One disadvantage with fluorescent tracers is the problem of photo bleaching (Shaner et al., 2005). As both fluorescent tracers and fluorescent immunohistochemistry were used in this study, steps were taken to minimize this problem by working quickly under the microscope and minimize the amount of light the sections were exposed to. All fluorescent sections were stored in the freezer and out of light in order to reduce bleaching.

The tracer Fluoro-Gold (FG) is one of the most commonly used tracers for retrograde tracing due to its high resistance to bleaching. It accumulates in lysosomes in the cytoplasm of the cell body, but can at higher concentrations fill the entire cell. Fastblue (FB) has many of the same qualities as FG, but labels the cytoplasm of the neuron. Both tracers can easily be visualized in the DAPI filter in the fluorescent microscope (Lanciego & Wouterlood, 2011).

Several other tracers were used during the course of this study, including Cholera Toxin subunit B, Diamidino Yellow and DiI. These tracers produce smaller injection sites and have a more narrow emission and excitation spectra compared to FB and FG, and were therefore used in order to get a more focused injection. Due to problems with transport from one or both injection sites, these experiments are not included in the result section.

2.4 Tissue collection

After surgery the animal was kept alive for approximately one week, before being weighed and anesthetized with Isoflurane. The animal was subsequently administered an intraperitoneal overdose of pentobarbital. After making sure that all reflexes and pain responses were absent, the animal was transcardially perfused, first with a ringer solution and subsequently with 4% paraformaldehyde in 125mM phosphate buffer. The brain was removed from the skull and post fixed in a paraformaldehyde solution (4%) overnight before being transferred to a container with DMSO (Phosphate buffer, 2% dimethyl sulfoxide and 20% glycerol) for cryoprotection and stored in the refrigerator until sectioning.

For sectioning, the brains were fixed with the dorsal side down on a freezing microtome (Microm HM430, Thermo Scientific, Waltham, USA) with a 30% sucrose solution. Crushed dry ice was used to maintain the brain in a frozen condition throughout the sectioning. The brains were cut in 50 µm thick horizontal sections, and collected in 6 series. The first series was mounted directly onto Superfrost Plus microscope slides (Gerhard Menzel GmbH, Braunschweig, Germany), while the remaining five series were put in cryoprotective containers containing DMSO and stored at -20 °C for further histology.

2.5 Immunohistochemistry

2.5.1. Reelin and Calbindin

Brains with good injection sites and transport were chosen for immunohistochemistry and subsequently stained for Reelin and Calbindin. The tissue was washed in 0.125M phosphate buffer for 3x15 minutes. Next, the tissue was washed in a phosphate buffer containing 0.5% Triton X-100 (Merck KGaA, Damstadt, Germany) for 3x15 minutes, before being blocked for three hours in phosphate buffer, containing Triton X-100 (0.5%) and normal goat serum (5%). Subsequently, the tissue was incubated with primary antibodies, mouse anti-Reelin (1:1000) and rabbit anti-Calbindin (1:5000) for 48 hours on a shaker in 4°C. Next, the tissue was washed with phosphate buffer (3x15), and incubated for 2-3 hours in room temperature with secondary antibodies goat anti-rabbit Alexa 546 (Invitrogen, Ltd., Paisley, UK) and goat anti-mouse Alexa 488 (Invitrogen, Ltd., Paisley, UK). Finally, the tissue was rinsed in phosphate buffer (3x15 minutes) and mounted on microscope slides (Menzel glass slide, Gerhard Menzel GmbH, Braunschweig, Germany) from 0.2% gelatine. The slides were dried for approximately 12 hours, cleared in Toluene and coverslipped using entellan as mounting medium. The full protocol, solutions and details on antibodies can be found in Appendix III and IV.

2.5.2. Calretinin

Several tests were performed in order to boost the quality of calretinin staining. All tests will be outlined in the result section below. The primary antibody used was mouse anti Calretinin (1:800) from Merck Millipore (Billerica, MA, USA) and the secondary antibody was goat anti-rabbit conjugated to Alexa 546 (Invitrogen, Ltd., Paisley, UK). All solutions, details on antibodies, and test protocols can be found in Appendix III and IV.

2.5.3. Green fluorescent protein (GFP)

A standard immunohistochemical staining procedure was performed in order to enhance the GFP signal in the mice brains (for details, see Appendix III). To avoid cross talk with Fastblue and Fluoro-Gold in

the microscope, the secondary antibody goat anti-guniea pig conjugated to alexa 546 (Invitrogen, Ltd., Paisley, UK) was used.

2.5.4. Cresyl Violet

To accurately delineate cytoarchitectonical borders, one adjacent series from each brain used for immunohistochemistry was stained with Cresyl Violet (Sigma-Aldrich, St. Louis, USA). Sections mounted on superfrost plus slides (Gerhard Menzel GmbH, Braunschweig, Germany) was rehydrated for approximately 2 minutes in distilled water, before being dehydrated with graded baths of alcohol. The tissue was subsequently cleared in xylene and rehydrated, before being placed in a Cresyl Violet solution for 3-8 minutes. The length of incubation varied depending on the tissue quality and the age of the solution and was therefore monitored. Excess colour was removed by alternating between running water and 70% ethanol containing acetic acid. Before coverslipping, the tissue was again dehydrated and cleared in xylene. The full protocol can be found in Appendix III.

2.6 Data analysis

2.6.1. Microscopy

All sections were analysed using a fluorescent microscope (Axio Imager M2, Carl Zeiss MicroImaging, Jena, Germany). Cases with good injections were chosen for further analysis using Neurolucida 10 (MBF Bioscience MicroBrightfield Inc.).

2.6.2. Neurolucida

Neurolucida was used to outline all sections of the relevant cases. As no cytoarchitectonic borders can be seen in the fluorescent microscope, a general outline of the cortex was made. Subsequently a general outline of MEC was drawn to ensure that the entire region would be covered. A meander scan was used to systematically scan through the entire outline. This was done under 40-x magnification, and each visible cell body was marked with a specific marker indicating what the given cell was positive for. By carefully plotting all labelled cells using Neurolucida the pattern of labelling could be analysed in detail without risk of bleaching the tissue. Once all sections had been scanned, Neurolucida Explorer (MBF Bioscience MicroBrightfield Inc.) was used to adjust size and colour of markers, and each section was subsequently exported separately for further analysis. Images of relevant cases were taken during analysis, however some images had to be taken later on in the analysis process and some bleaching of the immunohistochemically labelled cells was evident here. However, FB and FG are both tracers known for their resistance to photo bleaching and no bleaching of these labelled cells were observed during analysis.

2.6.3. Delineation and illustrations

To accurately delineate the borders of MEC, sections stained with Cresyl Violet were digitized using a Zeiss Mirax Midi Scanner (Carl Zeiss MicroImaging). High resolution images of these sections were imported to Adobe Illustrator CS6 (Adobe Systems Inc.), where they were aligned with Neurolucida drawings of the adjacent sections from the same brain. Based on the cytoarchitectonic borders visible in the Cresyl Violet stained sections, the borders of MEC was adjusted in the exported Neurolucida drawings, and markers outside the borders were deleted.

The aligned and adjusted images from Adobe Illustrator CS6 were subsequently imported into Adobe Photoshop CS6 (Adobe Systems Inc.). Here all images from one series were cropped into small zoomed in images of MEC and organized into one figure with overview images indicating the dorsoventral location of each cropped image. Lastly, the figure was finalized by adding text.

2.6.4. Calculation of dorsoventral position

As the hippocampal formation and the parahippocampal region use different axes to describe the long axes of the regions (figure 1), a dorsoventral axis of the entire brain was calculated to accurately describe where the injection sites were located. The first series of each brain was mounted directly on glass during sectioning, so this series was used to calculate the total the dorsal to ventral dimension of the brain. As the rat brain was cut in 50µm sections in six series and the mice brain in 40µm sections in 5 series, each section in any given series is 300µm apart in the rat brain and 200µm apart in the mouse brain. The first dorsal section in the first series is set as 0µm, the next section as 300µm (rat) and 200µm (mouse), and so on throughout the brain.

As a different series was used for analysis in Neurolucida, this was accounted for by adding the appropriate number of µm to each section depending on which series was used. For example, in series 3, the first section is located 100µm down the dorsoventral axis. In the results section, the descriptions of locations along the dorsoventral axis are made from the sections used for analysis with Neurolucida.

3. RESULTS

3.1. Rat experiments

3.1.1. Case 16957

Case 16957 had an injection of Fluorogold (FG) dorsally in the dentate gyrus of the left hemisphere. The main portion of the injection site is positioned approximately 2750µm ventral to the most dorsal section. Fastblue (FB) was injected in the dorsal MEC in the right hemisphere. The injection is located in superficial layers with some labelling in deeper layers. The dorsoventral location of this injection site is also approximately at 2750µm ventral to the most dorsal section.

Following injection of FB in dorsal MEC, fluorescently labelled FB cells were present in contralateral MEC. All labelled cells were located in the superficial layers, LII-LIII of MEC. No retrogradely labelled FB cells were found in deeper layers (LV-LVI). The majority of labelled cells in the contralateral MEC were located in the same section as the injection site, with some labelling extending approximately 300µm in both dorsal and ventral directions. A few labelled cells (6) were located more even ventrally, approximately 600µm from the level of the injection site. Four fluorescently labelled cells were found as far as 1800µm ventral to the injection site. The extent of labelling in MEC can be seen in Figure 6A-H, with the majority of the labelling in figure 6B. Total number of labelled cells is shown in graph 1.

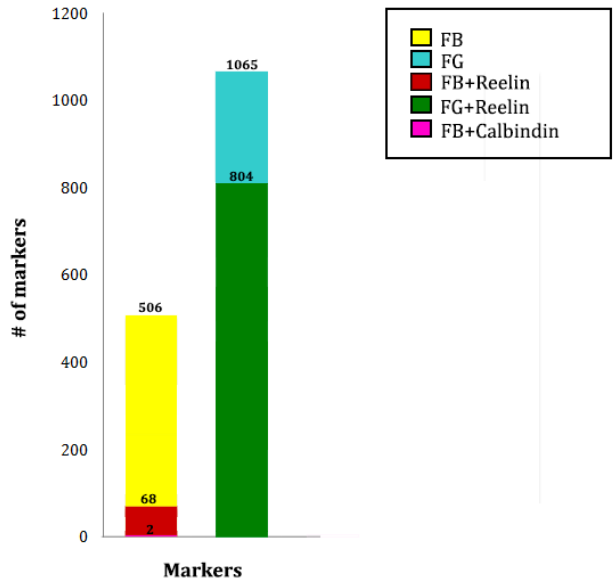

Graph 1: Number of retrogradely labelled cells in MEC following injection of FG in dorsal dentate and FB in dorsal MEC. Colocalization of retrogradely labelled cells of both classes with reelin and calbindin is shown as well.

An injection of FG in dorsal DG resulted in fluorescently labelled FG cells in the ipsilateral MEC. The labelled cells could be visualized as containing small yellow punctate or as intensely stained white cells depending on the amount of tracer taken up by the cell. The majority of labelled cells were located in superficial layer II of MEC. Some labelling was also located in the lateral part of MEC LIII. A few labelled cells could be found in deeper layers of MEC. The majority of labelled cells were located approximately 900µm along the dorsoventral axis, but labelling extend as far as 2100µm down. Figure 6A-H shows the labelling throughout MEC, with the majority of FG transport located in 6C-D.

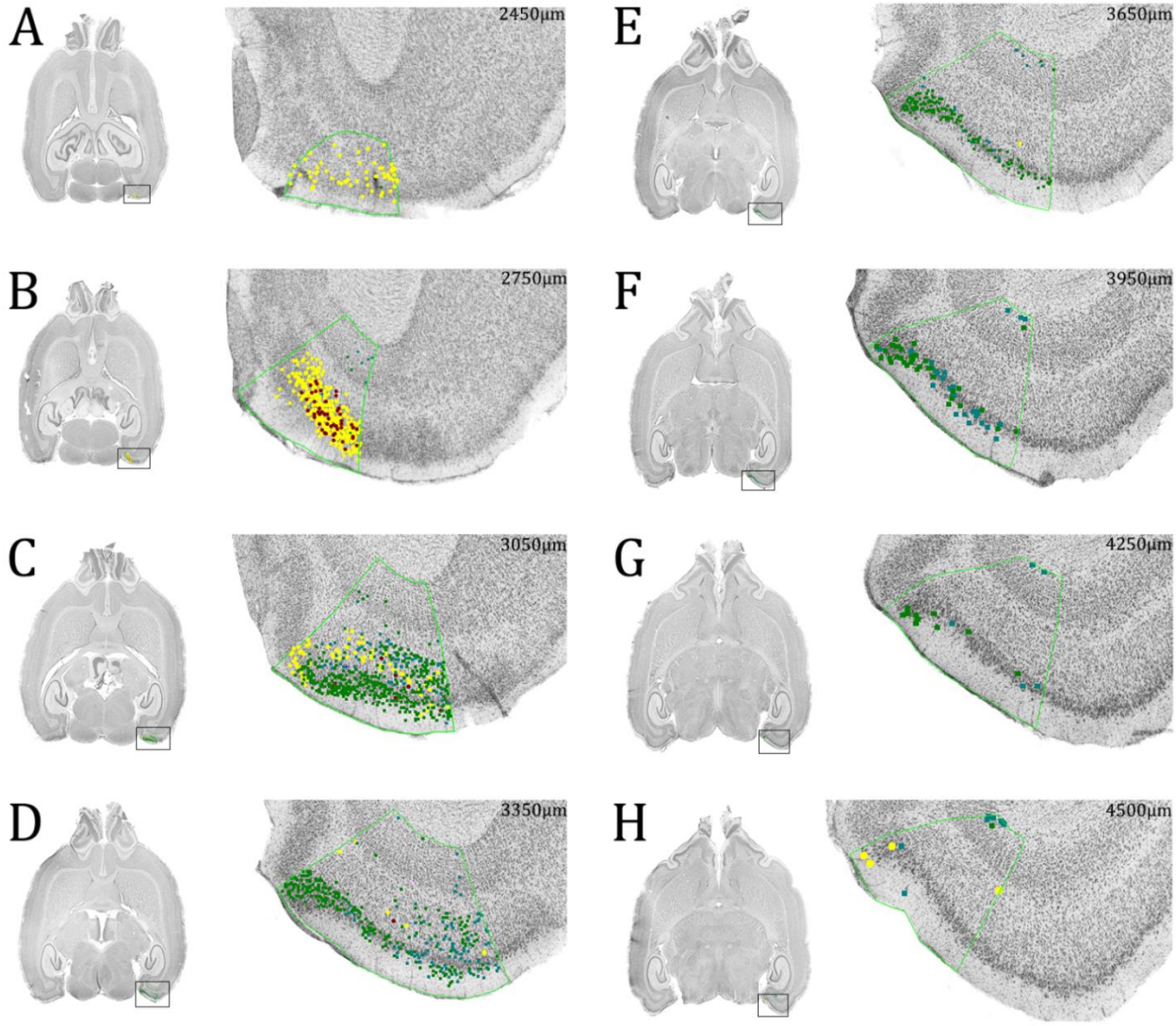

Figure 6: Retrogradely labelled EC projecting FB cells and DG projecting FG cells and colocalization with Reelin and Calbindin immunoreactive cells throughout the dorsoventral (A-H) extent of MEC. *Yellow:* EC projecting FB immunoreactive cells, *Red*: EC projecting FB+Reelin immunoreactive cells, *Pink:* EC projecting FB+Calbindin immunoreactive cells, *Blue:* DG projecting FG immunoreactive cells, *Green:* DG projecting FG+Reelin immunoreactive cells

Although no systematic measurements have been carried out, DG projecting FG labelled cells appear to have larger somata than EC projecting FB labelled cells. DG projecting cells also appear to have more neurites radiating from the cell body than EC projecting cells. Figure 7 illustrates the difference between the two labelled cells types.

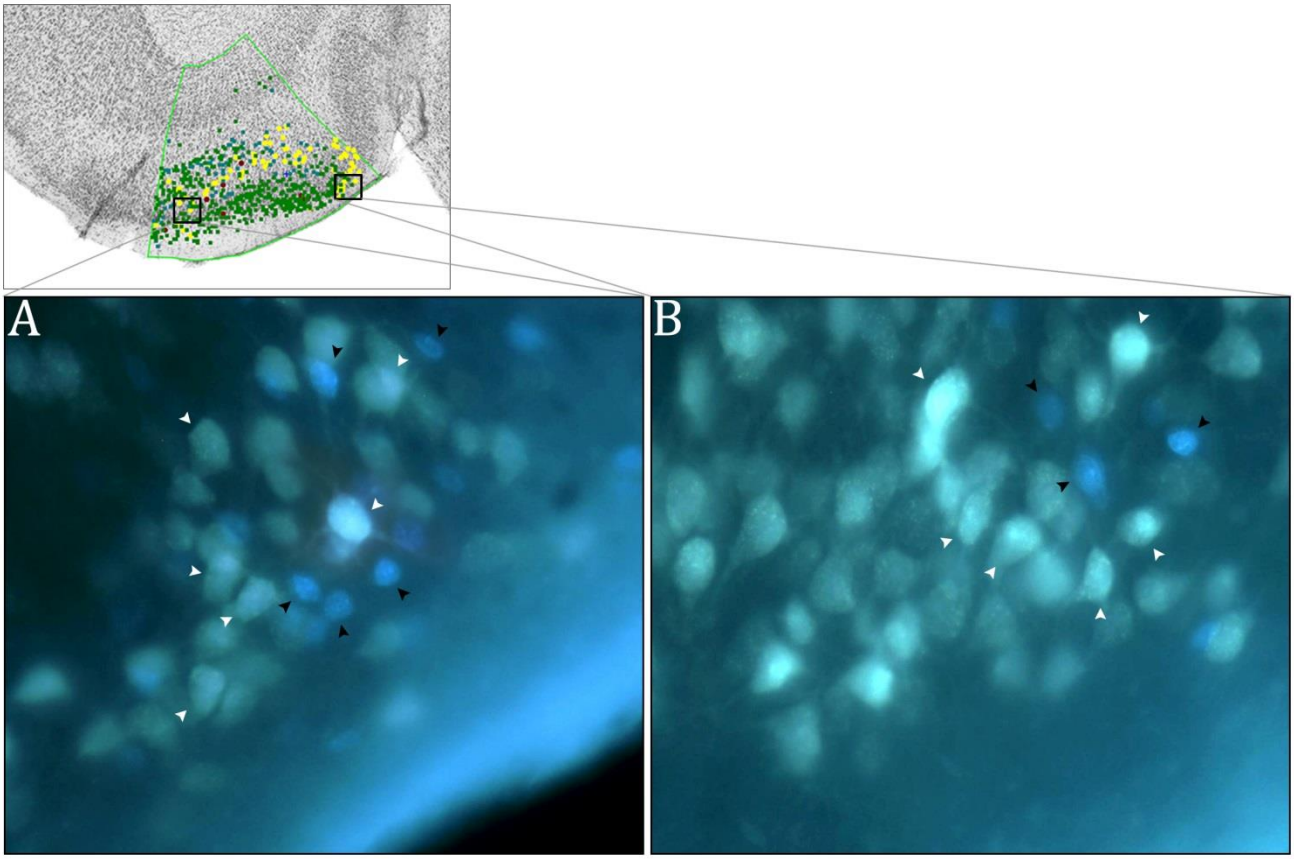

Figure 7: Retrogradely labelled DG projecting FG cells and EC projecting FB cells in lateral (A) and medial (B) parts of MEC. *White arrows:* FG labelled cells projecting to dentate. *Black arrows:* FB labelled cells projecting to contralateral MEC.

The proteins reelin and calbindin were labelled immunohistochemically with alexa 488 and alexa 546, respectively. Cells immunoreactive for reelin colocalized with both EC projecting FB cells and DG projecting FG labelled cells. A total of 75% of labelled DG projecting FG cells showed immunoreactivity for reelin, while 13% of the EC projecting FB positive cells showed reactivity for reelin. The majority of DG projecting FG cells immunoreactive for reelin was located in LII of MEC, although some labelled cells were present in the lateral part of LIII of MEC. The single DG projecting FG cells in LII appeared to be scattered throughout the layer, while in LIII the majority of single DG projecting FG labelled cells were located in the lateral portion of MEC. The majority of EC projecting FB cells immunoreactive reelin was located at the level of the injection site in both LII and LIII, with a few cells located 300 µm ventral to the injection site. The pattern of labelling can be seen in figure 6.

Calbindin immunoreactive cells showed little colocalization with either EC projecting FB or DG projecting FG labelled cells, but would often form a circle around cells retrogradely labelled from DG. Two EC projecting FB cell were found to be immunoreactive for calbindin, one of these can be seen in figure 8.

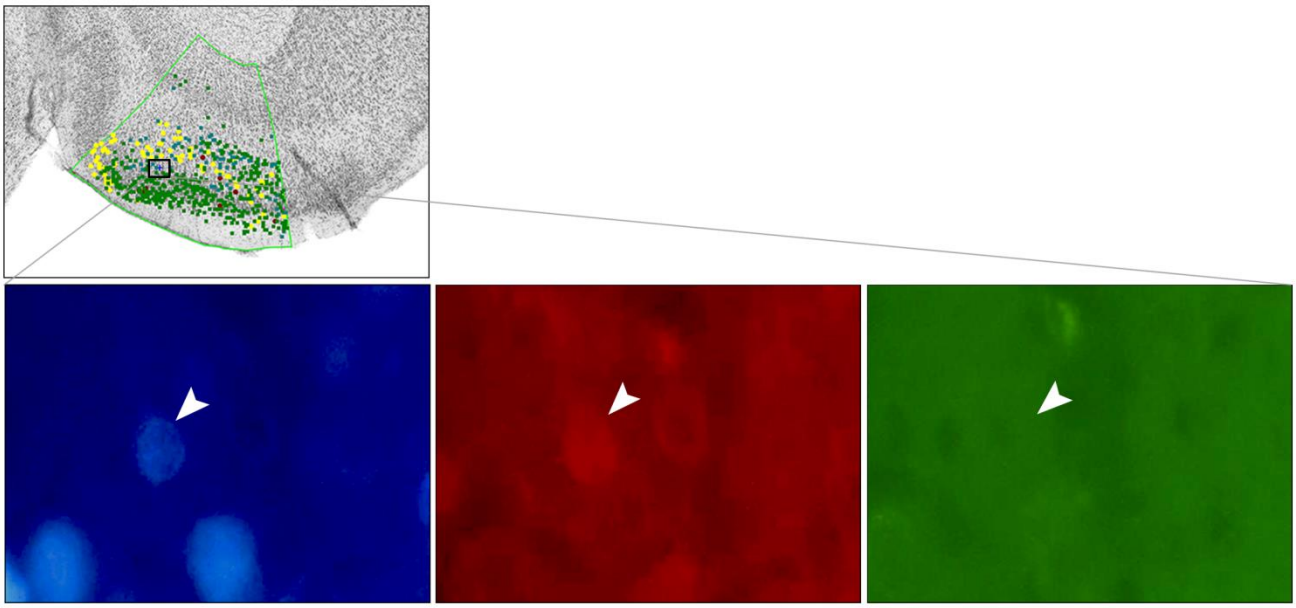

Figure 8: Retrogradely labelled EC projecting FB cell in medial part of MEC, immunoreactive to calbindin but not reelin. A: EC projecting FB labelled cells, calbindin positive cell indicated with white arrow. B: Cell positive for calbindin (White arrow). C: No cell body visible in the reelin filter (White arrow).

3.1.2. Case 16698 Calbindin

Case 16698 had an injection of Fastblue (FB) in dorsal MEC in the left hemisphere and an injection of Fluorogold (FG) covering the dorsal part of dentate (DG) and CA3 in the right hemisphere. The core of the injection site in MEC was positioned approximately 2500µm ventral along the dorsoventral axis, while the dorsoventral location of the injection in DG was at approximately 2000µm. The injection site in dorsal MEC covered the entire deep to superficial axis. The proteins reelin and calbindin were labelled immunohistochemically with alexa 488 and alexa 546, respectively.

In Case 16957 an injection of FG in dorsal DG labelled cells located mainly in LII of MEC. These cells did not colocalize with calbindin. The overall pattern of labelling in case 16698 was comparable to the one seen in case 16957, I did not observe colocalization with Calbindin and cells retrogradely labelled from DG. Therefore, I did not plot and count the FG labelled cells in this case.

Following an injection of FB in dorsal MEC, fluorescently labelled FB cells were present in contralateral MEC. The majority of labelled cells were located in the same section as the injection site, with some labelling extending approximately 300µm dorsal to the core of the injection and as far as 900µm ventral. The majority of labelled cells were located in layer III, while some cells were found in layer II and a few in superficial layer V. At levels dorsal to the site of injection, labelled cells are mainly located in LII and LIII, while in more ventral sections, most of the labelled cells are located in LIII (Figure 9A-E).

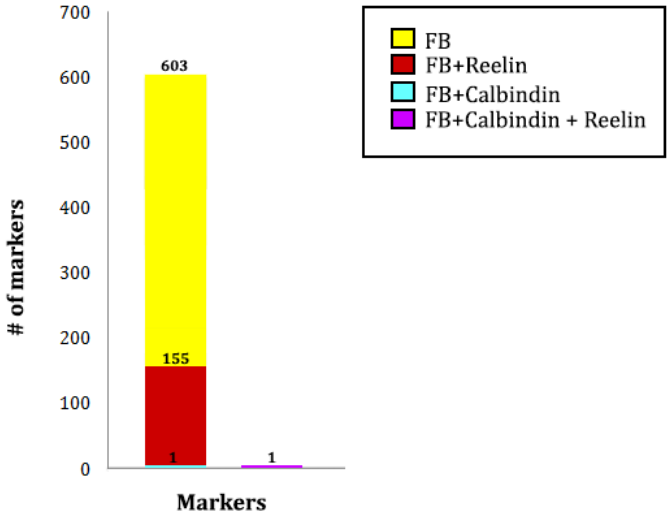

Graph 2: Number of retrogradely labelled cells in MEC following injections in dorsal MEC. Colocalization of retrogradely labelled cells with reelin and calbindin is shown as well.

A total of 25% of EC projecting FB labelled cells were found to colocalize with Reelin. These EC projecting FB and Reelin positive cells were scattered throughout LII – LIII of MEC. One cell was found approximately 600µm from the level of the injection site showing reactivity to both reelin and calbindin (Figure 10). One EC projecting FB positive cell was found to colocalize with calbindin but not with reelin. This cell and its position in MEC can be seen in figure 11. The total number of labelled cells in case 16698 CB can be found in graph 2.

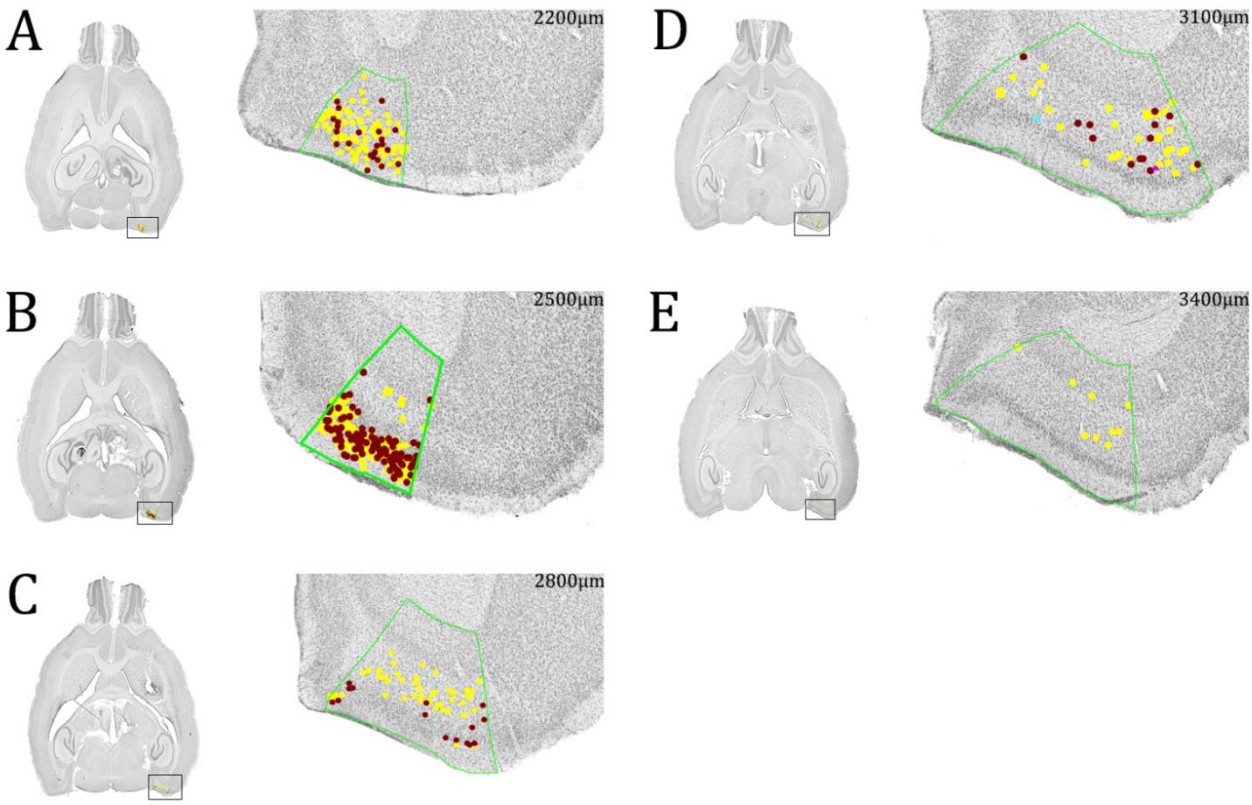

Figure 9: Retrogradely labelled EC projecting FB cells and colocalization with reelin and calbindin immunoreactive cells throughout the dorsoventral (A-E) extent of MEC. *Yellow:* EC projecting FB immunoreactive cells, *Red:* EC projecting FB+Reelin immunoreactive cells, *Turquoise:* EC projecting FB+Calbindin immunoreactive cell, *Pink:* EC projecting FB+Calbindin+Reelin immunoreactive cell

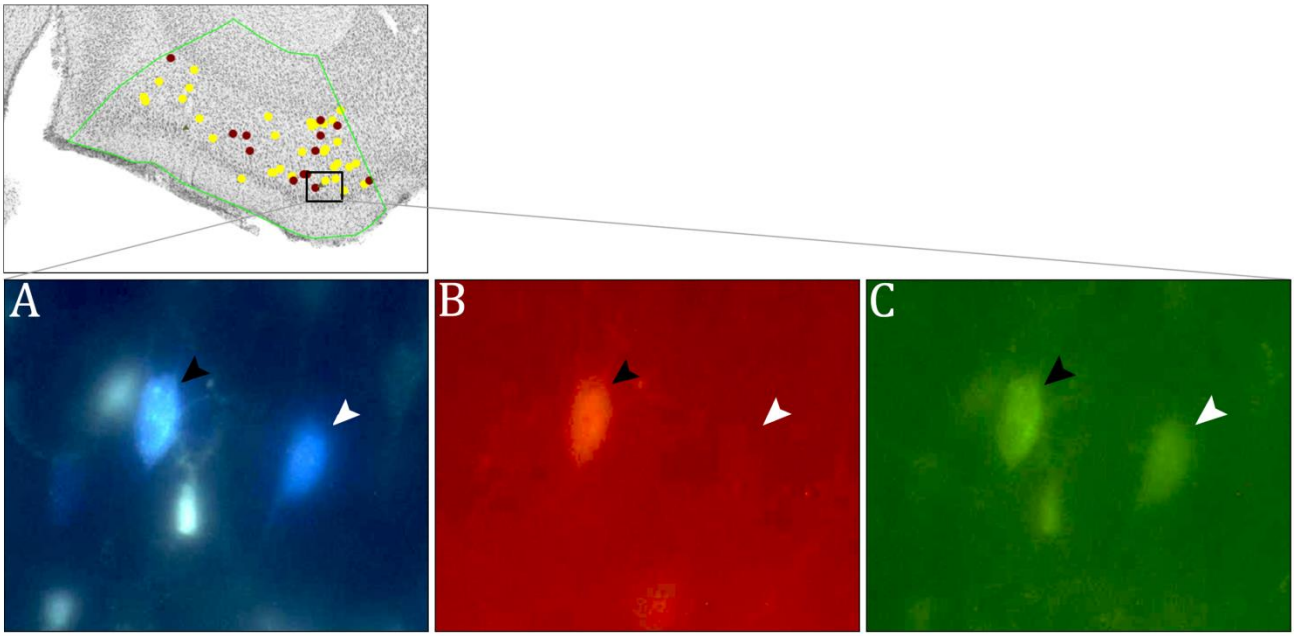

Figure 10: Retrogradely labelled EC projecting FB cell in lateral part of MEC, immunoreactive to both reelin and calbindin. *Black arrow:* EC projecting FB cell positive for both markers. *White arrow:* EC projecting FB cell positive for reelin, but not calbindin. A: EC projecting FB cells (black and white arrow). B: Calbindin immunoreactive cell (black arrow). C: Reelin positive cells (Black and white arrows)

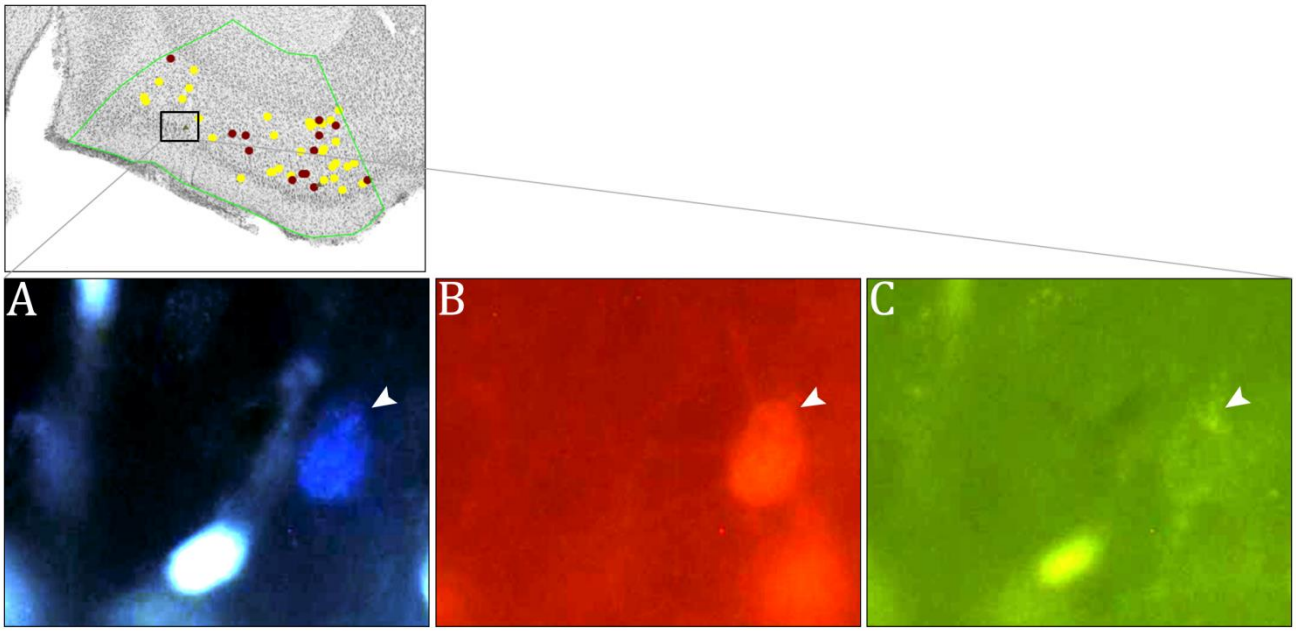

Figure 11: Retrogradely labelled EC projecting FB cell in medial part of MEC, immunoreactive to calbindin. White arrow: cell body. A: EC projecting FB labelled cell (White arrow). B: Same cell positive for calbindin (White arrow). C: No cell body visible in the reelin filter (White arrow)

3.1.3. Calbindin immunoreactivity in EC

In order to look at the expression pattern of calbindin throughout EC, sections stained for immunoreactivity to Calbindin have been overlaid with NeuN stained sections. As NeuN labels all neuron cell bodies, borders between layers and adjacent regions can be visualised.

Calbindin immunoreactive cells are located throughout the dorsoventral extent of EC (Figure 12A-X). The majority of labelling is located in deep LII of EC, with the densest labelling at mid dorsoventral levels. The labelling is not uniform throughout the EC, but rather forms patches of labelling along the mediolateral axis of EC. At the most medial border between MEC and parasubiculum as patch with very little labelling can be seen throughout the dorsoventral axis. Furthermore, labelling appears stronger in more lateral areas of EC, than medial regions. Some sparse labelling can be seen in deeper layers as well.

The pattern of labelling in fluorescent sections stained for calbindin with alexa 546 is comparable to the labelling described above.

Figure 12: Horizontal sections of rat EC. Immunoreactivity pattern of calbindin from dorsal to ventral (A-X), overlaid on sections stained for NeuN to visualize cell layers

3.1.4. CR tests

Series 4 of case 16698 was used to stain for the presence of calretinin (CR) (rabbit anti-Calretinin, Merck Millipore) in cells in MEC. This revealed a large amount of unspecific staining in addition to labelled CR neurons (fig 13 A and B). Labelled CR neurons could be separated from the unspecific labelling by the presence of labelled neurites. The unspecific labelling appeared as weakly labelled circular somata, without labelled neurites. The difference between unspecific labelling and a labelled CR cell can be seen in figure 13A, while figure 13B shows labelled CR neurons without unspecific labelling. As the unspecific labelling made it difficult to visualize weakly stained CR neurons, a number of tests were performed in order to eliminate or reduce unspecific labelling.

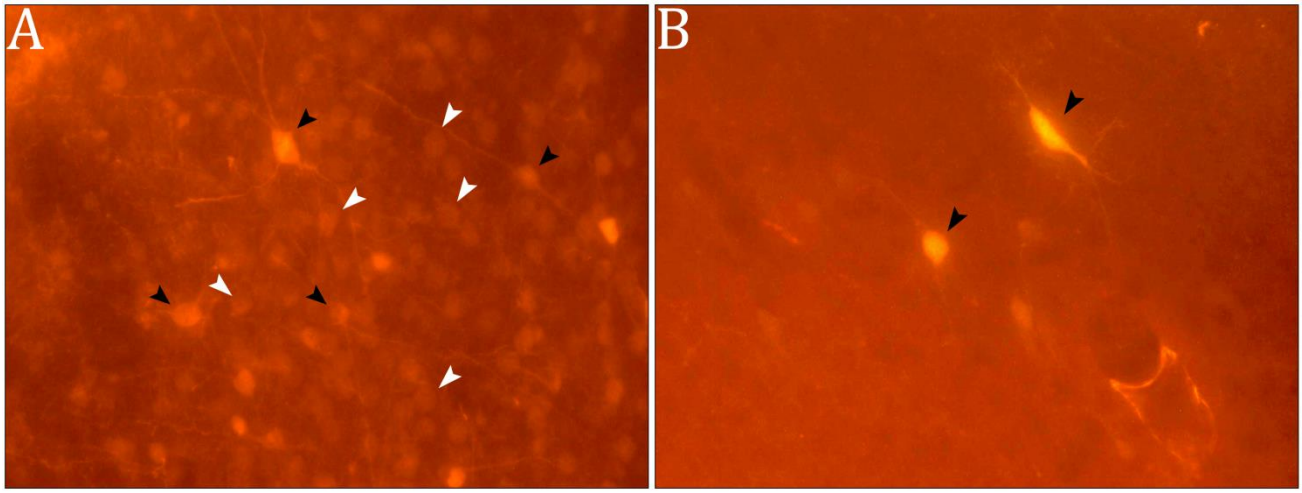

Figure 13: Specific and unspecific labelling of calretinin. A: Rabbit anti-Calretinin with unspecific staining. B: Mouse anti-Calretinin with no unspecific staining. *Black arrows:* Calretinin positive neurons. *White arrows:* Unspecific labelling.

First, a test of the secondary antibody was carried out in order to eliminate this as the reason for the unspecific labelling. The test was performed in one series from 16698 and one series from a different brain, 16935. This was done in order to rule out that the unspecific labelling seen in the previous CR staining was a result of problems with one specific brain. These tests did not yield unspecific labelling (Figure 14C and D). Next the incubation time with the primary antibody was reduced from 48 hours at 4° C to two hours in room temperature. This resulted in reduced unspecific labelling, but also fewer CR labelled neurons (Figure 14E and F). Thirdly, an absorption test was performed. Rat brain tissue was incubated with the primary antibody for 48 hours at 4° to allow the unspecific component of the antibody to bind to this tissue. Next, the primary antibody solution was pipetted out and used to incubate a new series of experimental sections. This resulted in similar unspecific labelling as seen in the original CR stain, with labelled CR neurons visible by the presence of neurites (Figure 14G and H).

Two blocking tests were performed in order to rule out that the blocking agent used for the previous CR staining and the different tests caused unspecific labelling. As the blocking agent used in the general immunohistochemical protocol was normal goat serum, tests with superblock and bovine serum as blocking agents were carried out. Both tests resulted in the same unspecific staining and labelling of CR neurons as seen when normal goat serum was used as the blocking agent (Figure 15A-D). A new batch of primary was ordered from Manufacturer, in order to rule out a problem with that specific batch of primary antibody. The same protocol as used for the original staining was used to ensure that all other variables were kept constant. This test also resulted in the same unspecific labelling as seen in the original staining (Figure 15E-F). Lastly another primary antibody (mouse anti-Calretinin) was obtained from Merck Millipore. This antibody had previously been used by Wouterlood et al (2007), which reported good CR labelling. As they had used a significantly different protocol than the one used in this thesis, tests were performed comparing the labelling that resulted using the two protocols. Both protocols labelled CR neurons and neither of the two tests showed the unspecific labelling reported above (Figure 15G-J). As no significant difference could be seen between the two protocols, the protocol used for the other immunohistochemical staining in this thesis was chosen for further CR staining. The full protocols for all tests can be found in Appendix III.

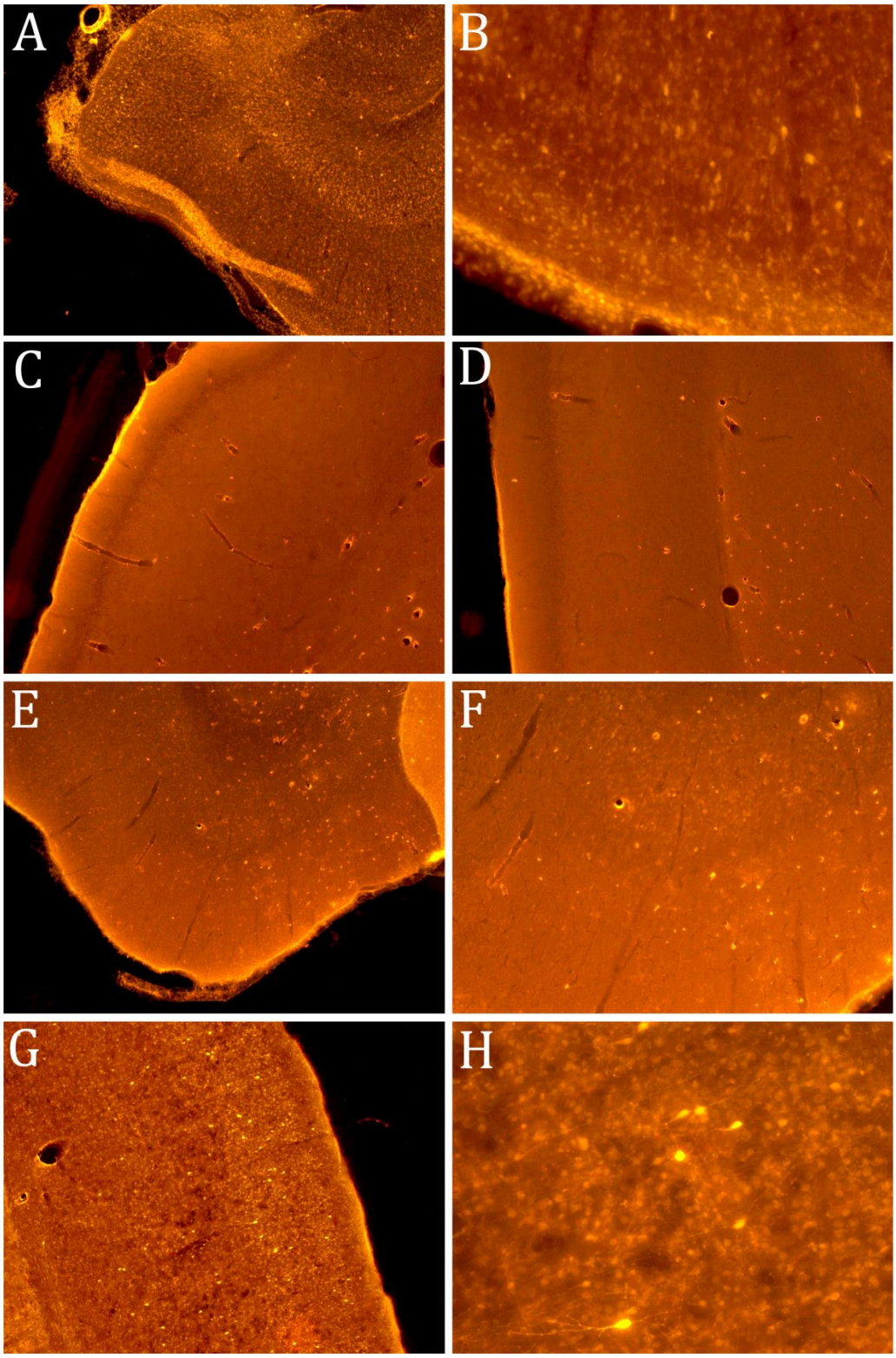

Figure 14: Unspecific labelling of Calretinin. A-B: The original CR staining revealing unspecific labelling (A: 5-x magnification, B: 20-x magnification). C: Secondary test with sections from 16698 (5-x magnification). D: Secondary test with sections from 16935 (5-x magnification). E-F: Test of shorter incubation time with primary antibody (E: 5-x magnification, F: 10-x magnification). G-H: Absorption test (G: 5-x magnification, H: 20-x magnification).

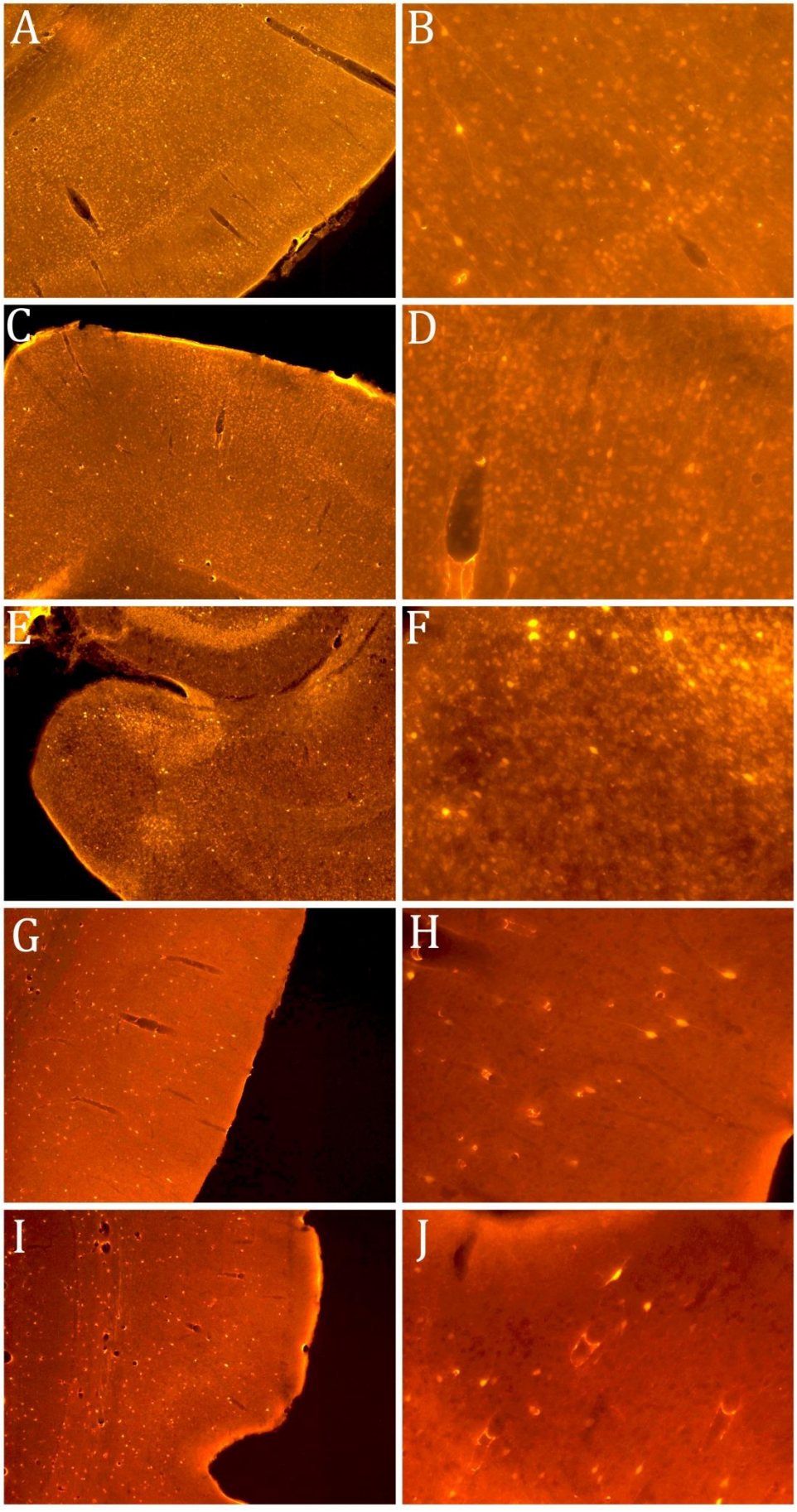

Figure 15: A-B: Blocking test with bovine-serum (A: 5-x magnification, B: 20-x magnification).

C-D: Blocking test with superblock (C: 5-x magnification, D: 20-x magnification).

E –F: New batch of primary antibody (E: 5-x magnification, F: 20-x magnification).

G-H: Test with mouse anti – CR, 72 hour incubation (G: 5-x magnification, H: 20-x magnification).

I-J: Mouse anti – CR, general protocol, 48 hour incubation. (I: 5-x magnification, J: 20-x magnification)

3.1.5. Case 16698 Calretinin

The injection sites in dorsal MEC and dorsal DG in Case 16698 have already been described in section 3.1.2. and will therefore not be described here. The protein Calretinin (CR) was labelled immunohistochemically with alexa 546.

The injection of FB in MEC resulted in fluorescently labelled FB cells in contralateral MEC. The majority of labelled cells were located in superficial layers, LII-LIII. Labelling extended approximately 300µm dorsal to the injection site and 900µm ventral from the level of the injection site. At the level of the injection site, the majority of labelled cells appeared to be located in LII-LIII, while at more ventral levels, the labelling appear to be localized mainly to LIII (Figure 16A-D).

Following the injection of FG in dorsal DG and CA3, fluorescently labelled FG cells were present in the ipsilateral MEC (Figure 16A-H). The cells were visible as containing small yellow puncta or as intensely stained white cells depending on the amount of tracer taken up by the cell. The majority of DG projecting FG labelled cells was located in LII, creating a clearly labelled band of cells covering both medial and lateral portions of MEC. This labelling was present as far as 1200µm ventral to the injection site. In even more ventral sections (1500- 1800µm), sparse labelling was visible in LV-LVI. The total number of labelled cells in each section of the brain can be found in Appendix I.

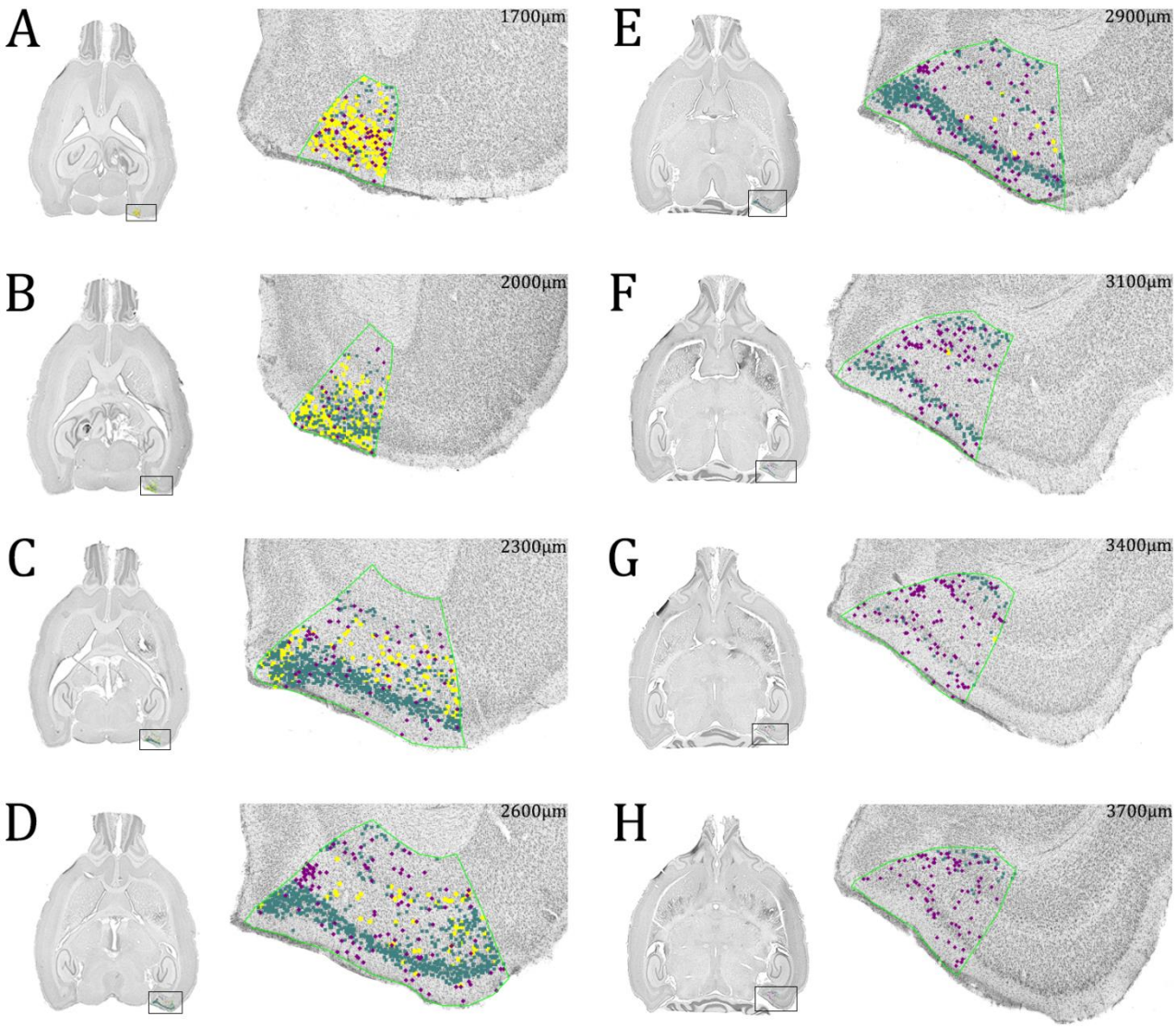

Figure 16: EC projecting FB cells, DG projecting FG cells, and Calretinin immunoreactive cells throughout the dorsoventral (A-H) extent of MEC. *Yellow:* EC projecting FB immunoreactive cells, *Blue:* DG projecting FG immunoreactive cells, *Purple:* Calretinin immunoreactive cells.

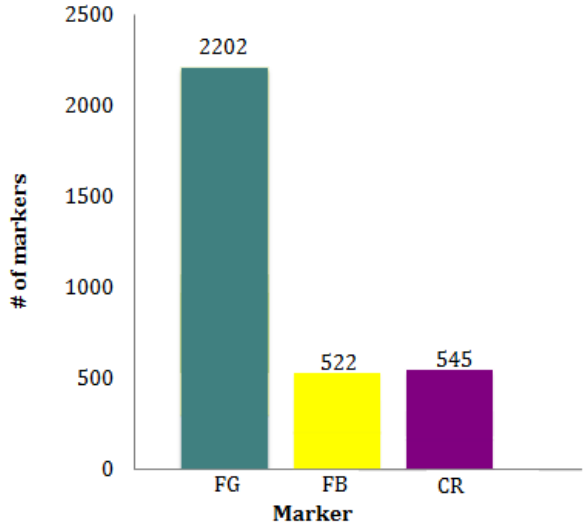

Graph 3: Number of retrogradely labelled FG and FB cells in MEC after injections in dorsal dentate and dorsal MEC. Number of CR immunoreactive cells is shown as well.

Cells immunoreactive for Calretinin appear to be scattered throughout the entire dorsoventral extent of MEC. Though no clear pattern is visible with respect to dorsoventral location, a pattern does emerge with respect to the deep to superficial axis. Although no quantifications have been made, more CR immunoreactive cells appear to be located in superficial layers (LI-LIV) than in deeper layers (LV-LVI). A clustering of immunoreactive cells was found in the medial part of LIII, situated close to the border between MEC and parasubiculum. This patch of cells can clearly be seen in figure 16D-E. Neither EC projecting FB cells, nor DG projecting FG positive cells showed colocalization with Calretinin (Graph 3).

3.2 Mice experiments

In order to investigate if any of the cells projecting to contralateral MEC were GABAergic, injections in dorsal MEC and dorsal DG were done in GAD67-GFP positive mice. As this transgenic mouse strain expresses green fluorescent protein (GFP) in neurons containing GAD67, cells with this marker are fluorescently labelled green. Two representative cases will be outlined below.

3.2.1. Case 2413

Case 2413 has an injection of FG in superficial layers of dorsal MEC in the left hemisphere. The core of the injection site was positioned 1640µm down to the dorsal surface of the brain. The right hemisphere has an injection of FB in the dorsal DG, with the core of the injection located approximately 1640-1840µm along the dorsoventral axis. Additional immunohistochemical staining for GFP was done to enhance the labelling using a red fluorophore (alexa 546).

An injection of FB dorsally in DG resulted in fluorescently labelled FB cells in superficial layers of ipsilateral MEC (LI-LIII). The majority of labelled cells are located in LII, but at dorsal levels labelling is also visible in LIII (Figure 17B-C). Labelling tapers off at approximately 1800µm ventral to the injection site.

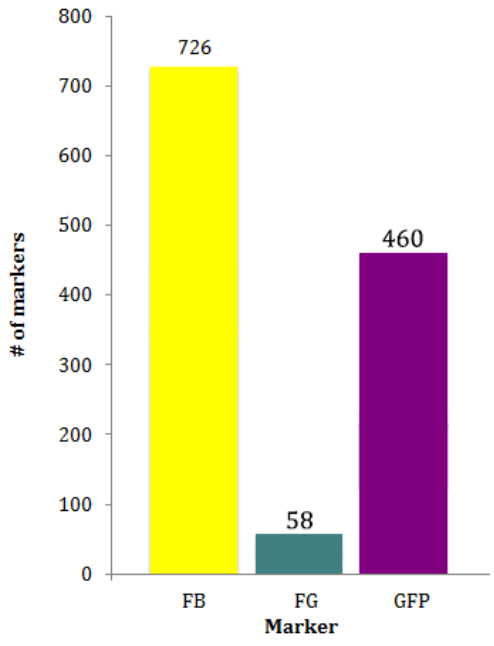

Graph 4: Number of retrogradely labelled cells in MEC following injections in dorsal dentate and dorsal MEC. Number of immunoreactive GFP cells is shown as well.

Following an injection of FG in dorsal MEC, fluorescently labelled FG cells were present in the contralateral MEC. The labelling is quite sparse, spreading approximately 300µm dorsally, and no apparent spread ventrally. Labelled cells were located in the medial part of MEC, close to the border between MEC and parasubiculum. The extent of labelling can be seen in figure 17, with the retrogradely labelled FG cells located in figure 17B.

Immunoreactive GFP cells were located throughout the dorsoventral and deep to superficial extent of MEC. No apparent pattern of labelling was visible. Immunoreactive GFP cells colocalized with neither DG projecting FB cells nor EC projecting FG labelled cells (Graph 4).

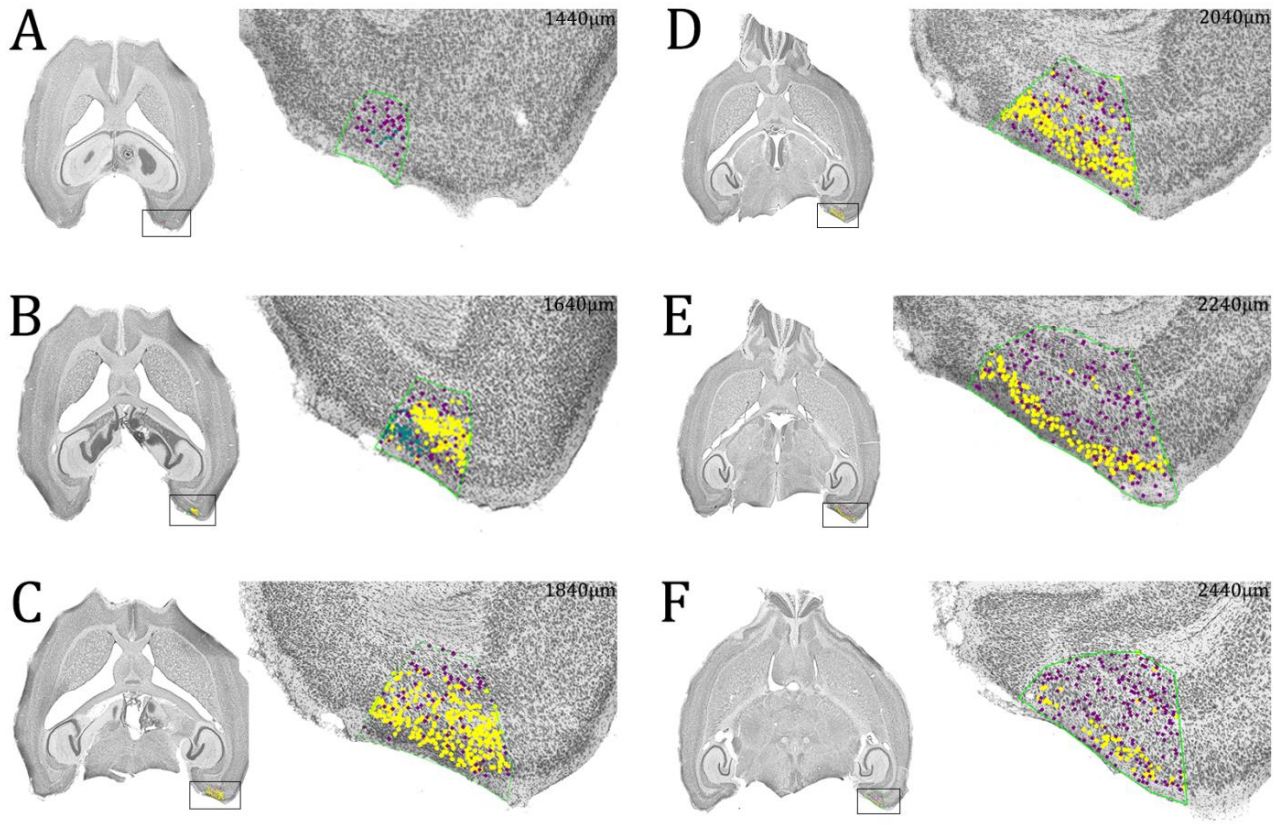

Figure 17: EC projecting FG cells, DG projecting FB cells and GFP immunoreactive cells throughout the dorsoventral (A-F) extent of MEC. *Yellow:* DG projecting FB immunoreactive cells, *Blue:* EC projecting FB immunoreactive cells, *purple:* GFP immunoreactive cells.

3.2.2. Case 2628:

Case 2628 has an injection of fastblue in superficial layers of dorsal MEC in the left hemisphere. The core of the injection site is positioned 1640µm along the dorsoventral axis. As for the case described above immunohistochemical staining for GFP was performed in order to enhance the labelling using a red fluorophore (alexa 546).

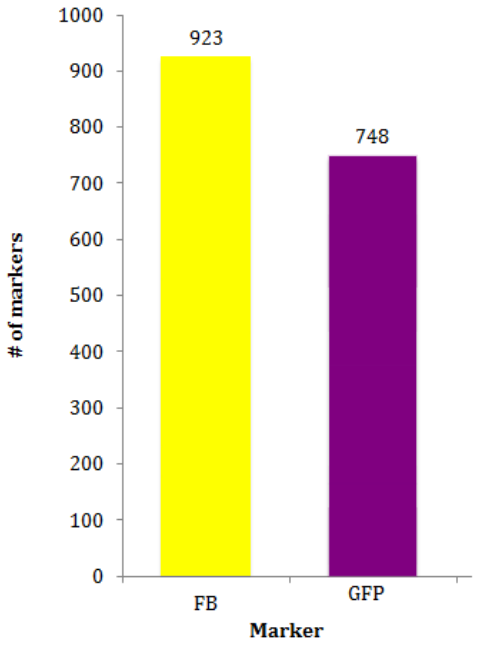

Graph 5: Number of retrogradely labelled cells following an injection in dorsal MEC and number of GFP immunoreactive cells.

After injection of FB in superficial layers (LI-LIII) of dorsal MEC, fluorescently labelled FB cells were present in contralateral MEC. All labelled cells were confined to the superficial layers of MEC with the majority of the labelled cells in LIII. At dorsal levels labelled FB cells were located in both LII and LIII, while at more ventral levels the labelling was located only in LIII. GFP positive cells were found scattered in all six layers of MEC in all dorsoventral levels. Figure 18A-G shows the labelling throughout MEC. Similar to the previously described case, EC projecting FB labelled cells did not colocalize with GFP positive cells. The total number of labelled cells in case 2628 is plotted in graph 5.

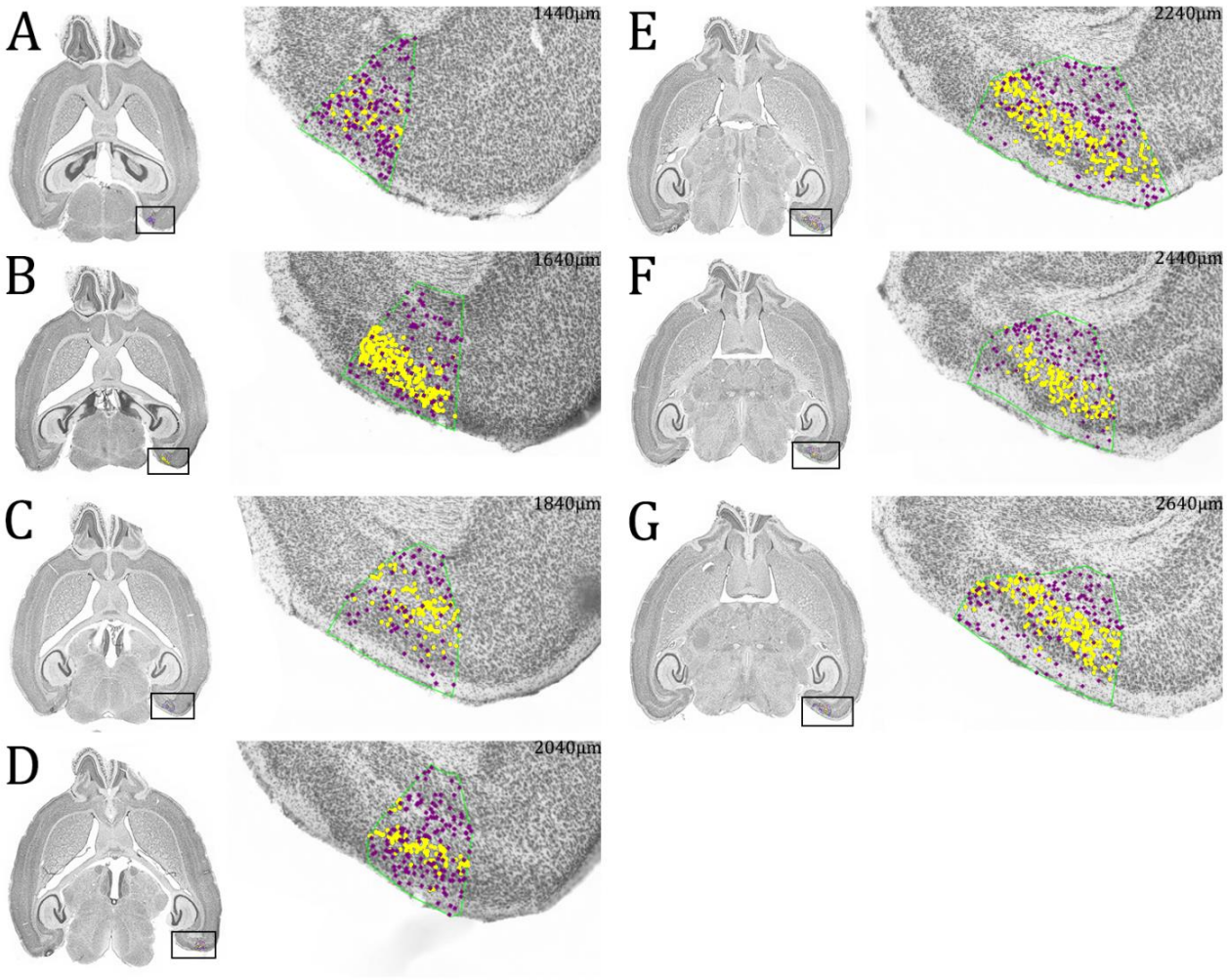

Figure 18: EC projecting FB cells and GFP immunoreactive cells throughout the dorsoventral (A-F) extent of MEC. *Yellow:* EC projecting FB immunoreactive cells, *purple:* GFP immunoreactive cells.

4. DISCUSSION

4.1. Summary of main findings

The purpose of this thesis was to investigate the specificity of output from cells in superficial layers of MEC. The results presented here indicate the presence of at least three separate cell populations. Cells in LII which contribute to the perforant path projection to DG appear to be mainly stellate-like in morphology. Three quarters of the cells contributing to this projection were found to express reelin. A second population of cells expressing calbindin resides in deep LII of MEC. The projection pattern of this population is still unknown. The third population of cells can be found in LIII of MEC, making up the commissural projection to contralateral MEC. The morphology of these cells appears to be pyramidal-like, and while the expression pattern of this projection remains largely unknown, a part of the population was found to express reelin. Figure 19 shows a schematic representation of the results.

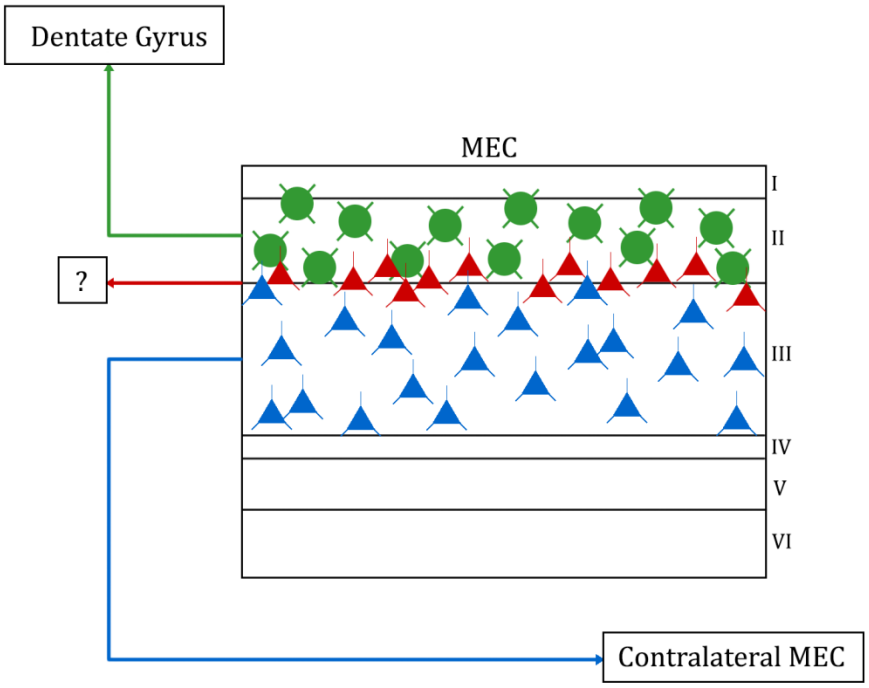

Figure 19: Schematic summary of main findings. *Green cells:* Reelin positive stellate cells projecting to ipsilateral DG. *Red cells:* Calbindin positive cell population with unknown projection targets. *Blue cells:* Commissurally projecting pyramidal cells with unknown chemical markers.

4.2. Methodological considerations

A few aspects of the methods in this study should be taken into consideration. Firstly, anatomical tract-tracing techniques have some limitations. Though a large amount of tracer was deposited in one area, this does not guarantee that all cells within this area are labelled or that all cells take up and transport the tracer. It is therefore not possible to fully exclude that there are cells within MEC with a different immunohistochemical profile and projection pattern than reported in this thesis.

Another disadvantage of fluorescent tracers and fluorescent immunohistochemistry is the problem of photo bleaching (Shaner et al., 2005). The steps taken to reduce bleaching of the tissue are outlined in the method section. All patterns of labelling were analysed in detail with the plots generated from Neurolucida. As these plots were generated by meticulously scanning through each section at 40-x magnification I am confident that the illustrations and analysis provide an accurate representation of the labelling seen in these brains.

All cell labelling was analysed with Neurolucida software. As this program does not set an upper and lower limit in the z-plane, extra care was taken to ensure that the z-plane was not adjusted more than necessary. For cells with possible colocalization every precaution was taken to ensure that it was in fact the same cell. As cells would often lie close together or seemingly on top of each other, indicating overlap, precaution was taken to ensure that the labelled cell was in fact double labelled by ensuring that the cell was in the same location in the x, y and z-plane in all relevant filters in the microscope. In order to generate more absolute numbers, a program like Stereo Investigator (MBF Bioscience) could have been used. Another option would be to use confocal microscopy as this allows for optical sectioning of the section and would yield information about the relationship of cells in the z- plane (Dailey et al., 1999). However, for the purpose of this thesis, it was more relevant to generate a general overview of the labelling pattern within MEC and the Neurolucida software was best suited for this task and the time frame of the project. Nonetheless, as mentioned above, special care was taken with regards to the z-plane in order to generate as accurate numbers as possible.

As indicated above, measures have been taken to reduce potential confounds and the possibility of false negatives and false positives. I am therefore confident that the results presented in this thesis are accurate.

4.3. Entorhinal – Dentate projection

The results show that stellate cells in LII of entorhinal cortex projects to the dentate gyrus. The projection neurons covered the majority of the medial-lateral axis and a substantial part of the dorsoventral axis of MEC. This projection pattern is in accordance with what has been previously reported (Witter & Amaral, 1989, Witter, 2007). Some cells in LIII of the more lateral part of MEC, were also seen to project, indicating that parts of the DG injection has bled over into the CA1 region (Witter et al., 1988).

A total of 75% of cells in MEC projecting to DG were found to be positive for reelin. In view of the finding that 67% of layer II cells are stellate cells (Gatome et al., 2010), one may assume that the stellate DG projection neurons are reelin positive, whereas the non-reelin positive remaining 25% are non-stellate DG-projecting neurons. However, the numbers of reelin expressing cells projecting to DG reported here are not as high as those reported by Varga et al (2010), who reported 100 % colocalization, i.e. all DG projecting neurons are reelin positive. This discrepancy could in part be caused by false negatives due to the strictness of plotting. Only clearly double labelled cells were included in the dataset in order to minimize the occurrence of false positives. The total percentage of colocalization can therefore be thought to be slightly higher than what is evident from the present results, it is however unlikely that the number of false negatives is as high as 25% of the cells. Thus, parts of the cell population projecting to DG appear to express a different chemical marker.

None of the cells projecting to DG expressed calbindin, which is in line with previously reported findings (Varga et al., 2010). However a few calbindin positive stellate cells in LII and pyramidal cells in LIII of EC have been reported (Witter & Wouterlood, 2002). This discrepancy in labelling patterns can be a result of antibody differences, or that these cells were not labelled in the present study. As mentioned in section 4.2. it is not possible to guarantee that all cells in a region take up and transport the injected tracer. As the number of reported calbindin positive cells in MEC projecting to dentate was small even in cases with a large retrograde injection in HPC (Witter & Wouterlood, 2002), it is possible that these cells just weren't labelled in this study.

4.4. Commissural MEC projection

The commissural MEC projection is a very focal projection where injection of a retrograde tracer in one area of MEC will label roughly a comparably sized homotopic area of contralateral MEC (Amaral & Lavenex, 2007). This projection arises mainly from LIII of MEC, which is in accordance with reports (Steward & Scoville, 1976). A few cells were found in LII as well, which is in line with reports from

Köhler (1986). As Köhler did not describe the amount of labelling in each layer it is difficult to compare those results with the results from this project. Nonetheless, it is clear that the majority of commissurally projecting cells are located in LIII of MEC. All commissurally projecting cells were pyramidal to multiform like in morphology. This is in accordance with the reported cell types in LIII of EC (Canto & Witter, 2011).

Very few of the commissurally projecting cells in MEC expressed calbindin. Out of 1109 cells, a total of three cells were found to express calbindin, while one cell expressed both reelin and calbindin. Furthermore, up to one fourth of all commissurally projecting cells expressed reelin. These results are in conflict with previous reports where the majority of all commissurally projecting cells are positive for calbindin while negative for reelin (Varga et al., 2010). The calbindin positive cells reported by Varga et al (2010) are located in LII of MEC. As the commissural projection arises mainly from LIII of MEC (Köhler et al., 1978, Steward & Scoville, 1976), it raises the question as to which cell population Varga et al have analysed.

All MEC injections in this project are restricted to dorsal levels, thus, it is not possible to exclude that the pattern of labelling reported by Varga et al (2010) can be found with injections in more ventral levels of MEC. Differences with regards to immunoreactivity to different chemical markers along the dorsoventral axis of MEC have been reported in the entorhinal cortex of adult mice (Fujimaru & Kosaka, 1996). It is therefore possible that this type of expression pattern can be found in the MEC of the rat as well. As Varga et al (2010) did not specify where in MEC they injected, I cannot exclude the possibility that injections along the entire extent of the dorsoventral axis of MEC would reveal a different and possibly more complex expression pattern than what is reported here.

Cells projecting to contralateral MEC did not colocalize with calretinin, a marker which have previously been found throughout the layers of EC. Furthermore, calretinin has been shown to not be expressed in cells projecting to DG. The labelling of calretinin seen here is comparable to previous reports of the expression pattern in EC (Wouterlood et al., 2000). A patch of calretinin expressing cells was found in LIII at the medial border between MEC and parasubiculum which was not mentioned in previous reports.

In order to address if parts of the commissural projection is GABAergic, labelling and colocalization in GAD67-GFP positive mice were analysed. Although no overlap between the commissurally projecting population and GAD67 was found, the scattered pattern of GAD-labelling throughout all layers of MEC is

comparable to the expression pattern reported in other studies (Köhler et al., 1985). As mentioned in section 4.2., this does not necessarily exclude the possibility that commissurally projecting MEC cells are immunoreactive for these markers as it is not possible to guarantee that all commissurally projecting cells were retrogradely labelled. Additionally, the lack of GAD67 expression in cells projecting to contralateral MEC do not exclude that commissurally projecting cells in MEC are GABAergic, as I did not do immunohistochemistry for GAD65, the other synthesising enzyme for GABA. The two markers are not similarly distributed within neurons or within brain regions, and while GAD67 is mostly found in cell bodies, GAD65 is mostly expressed in axon terminals (Esclapez et al., 1994). The distribution of the two markers within MEC has not been reported.

4.5. Calbindin immunoreactive cell population

The expression pattern of calbindin throughout the dorsoventral extent of EC has to this date not been fully described. The calbindin positive cell population is unevenly distributed along the mediolateral axis and appears to be located deep within LII and at the border between LII and LIII of EC. This is in line with previous reports, although calbindin labelling has also been reported in LIII of both MEC and LEC, with reportedly more abundant labelling in LEC compared to MEC (Witter & Wouterlood, 2002). It remains unclear why this pattern of labelling is not seen here. It could in part be caused by differences in antibodies or histochemical procedures, as it is not clear which antibody was used in the study. However, the one image shown from the study appears to have similar labelling to what is seen in this study, with labelling in deep LII and no labelling in LIII. This image is taken from MEC, and no comparable image from LEC is shown, making in difficult to fully compare the two studies. It is also not clear from the description where in LIII these calbindin positive cells were found, so one possibilty could be that the cells are located in superficial LIII, in line with observations decribed in this thesis.

The distribution of calbindin along the mediolateral axis appear to be organized in patches, which corresponds to previous reports (Witter & Moser, 2006). At the most medial border between MEC and parasubiculum, a patch of weak calbindin expression can be seen. This patch can be seen throughout the dorsoventral extent of MEC in varying amounts. Patches of functionally identified cells in MEC have been reported previously (Burgalossi et al., 2011), it is however unclear if these correspond to the patches of calbindin cells seen here.

The few calbindin positive cells found to project to contralateral MEC are all located at the border between the LII and LIII, therefore, they do not lend conclusive support to either side of the LII/LIII debate regarding commissurally projecting cells. Nonetheless, the calbindin immunoreactive cell

population do not colocalize to a large degree with the EC-DG projection or with the commissural projection. It is therefore not clear at this point where the calbindin-expressing population projects to. It does however not seem like the population is strictly an interneuron population like other calcium binding proteins (Miettinen et al., 1996) as only a small portion of calbindin positive cells have been reported to co-express GABA (Wouterlood & Jasperse, 2001). Additionally, although not replicated in this study, a few principal cells expressing calbindin in EC have been reported (Witter & Wouterlood, 2002). One possibility is that calbindin is expressed in the cells in LII of EC projecting to other areas of the brain like medial prefrontal cortex or olfactory structures (Insausti et al., 1997). As Varga et al (2010) made retrograde injections in the fimbria-fornix in order to verify that EC project commissurally, cells labelled from these injections might express calbindin. It is however known that the commissural EC projection pass through the dorsal hippocampal commissure, and not the fimbria-fornix. Cells projecting out through the fimbria-fornix therefore do not project to the contralateral EC, but rather to contralateral HF or other brain areas (Adelmann et al., 1996). If the data reported by Varga et al (2010) are from fornix injections rather than injections in contralateral MEC, this would explain the discrepancy between the results presented here and what Varga reports.

4.6. Functional implications

The EC-DG projection constitutes a major input from the entorhinal cortex to the hippocampal formation. A single stellate cell in LII of MEC have been shown to project to both DG and the HF by way of branching (Tamamaki & Nojyo, 1993). Functionally, it is believed that grid cells are necessary for the generation of place cells in the hippocampus, and that they are among the MEC cells projecting to the hippocampus (Bonnevie et al., 2013, Solstad et al., 2006, Zhang et al., 2013). Conversely, it has been shown that grid cells also require input from the hippocampus in order to maintain their gridness (Bonnevie et al., 2013).

The majority of cells projecting to DG were found to express the chemical marker reelin. This protein is known to be involved in neuronal migration in the developing brain and in synaptic plasticity (Borrell et al., 1999, Ramos-Moreno et al., 2006). It is expressed in many areas of the brain including the neocortex, the hippocampal formation, and the entorhinal cortex. Reelin has been found to be expressed in the whole entorhino-hippocampal pathway, including the cells of origin in LII of EC, the axons and terminal fields in HF (Ramos-Moreno et al., 2006). A lack of reelin results in misrouted fibres and abnormal patches of termination in the afferents from EC to HF, indicating that reelin is important in the formation of specific connectivity between the hippocampus and entorhinal cortex. However, this abnormal connectivity pattern was found to be caused by a lack of reelin in HF (Borrell et al., 1999). What function reelin has in EC is not yet known. One possible explanation is that reelin is involved in

the development of the network generating the functional grid pattern in LII of MEC. The cell network proposed to generate this grid pattern includes connections between interneurons and stellate cells in LII (Couey et al., 2013). It is conceivable that, similar to the role in guiding EC-DG projections, reelin in EC is necessary in order to guide and generate the network underlying the grid pattern. Furthermore, the amount of reelin in the brain is known to decrease progressively from postnatal week two when the majority of neuronal migration has completed (Soriano & Del Rio, 2005, Pesold et al., 1998). This drop in reelin appears to happen shortly before the grid network comes "online" and grid cells display adult like firing (Wills et al., 2012, Langston et al., 2010).

The functional implications of the commissural MEC projection have yet to be elucidated. However, as no stellate cells were observed to be retrogradely labelled from contralateral MEC, this suggests that the commissural projection could be made up of other functional cell populations, and not by grid cells. However, grid cells have been found in all layers of MEC, including layers without stellate cells, indicating that other morphological types can generate grid cell properties (Sargolini et al., 2006). In addition to grid cells, other functionally defined cell populations can be found throughout EC. The cells which fire in response to head direction are located in LIII, LV and LVI of MEC, while border cells have been found in all layers of MEC. Additionally, conjunctive cells, showing both head direction and grid cell properties are mostly located in LIII of MEC (Solstad et al., 2008, Sargolini et al., 2006).

To this date, no studies have been done to elucidate which morphological cell type corresponds to each of the functionally defined cell types in MEC. It is however possible to imagine that if most stellate cells are grid cells, perhaps other morphological cell types corresponds to other functional populations as well. If this were the case, based on the results presented here, it would open for the possibility that head direction cells and border cells project contralaterally, while grid cells do not. However, this does not account for the grid cells in LIII which have been shown to generate place cells in CA1 by way of a direct projection form LIII of MEC to CA1 (Brun et al., 2008a). As stellate cells can be found in LIII as well, it is possible that these cells correspond to the grid cells in LIII. This is in line with reports that the number of grid cells in LIII is quite low, as are the number of stellate cells in LIII (Sargolini et al., 2006, Canto & Witter, 2011). Nonetheless, grid cells have also be found in layers without stellate cells. Thus, is not possible to exclude that pyramidal cells in LIII corresponds to the grid cells in this layer, and if this is the case, that these grid cells contribute to the commissural projection as well. In addition to stellate cells, several types of pyramidal cells have been reported to exist in LIII of MEC (Canto & Witter, 2011). One possibility is that each of these morphological cell types corresponds to a different functionally defined cell type in LIII.

It has earlier been proposed that HF back-propagations ensure that the grid network do not accumulate errors over time and drift in self-positioning (Samu et al., 2009). However these back propagations are necessary to generate the grid pattern (Bonnevie et al., 2013). If the error and drift correction does not originate from the HF, how does the grid network avoid the accumulation of error and drift over time? Perhaps this stabilization comes from head direction and border cells in LIII of MEC projecting contralaterally. This falls in line with the model presented by Bonnevie et al (2013) where they show that grid cells get input from head direction cells. The grid pattern would be generated separately with input from ipsilateral HF back propagations, while the commissural projection would stabilize the networks so as to not generate errors and drift in self-position over time. As the commissural projection is known to be an incredibly focal projection, this stabilization would be done within each grid module (Stensola et al., 2012).

4.7. Future directions

The results presented in this thesis do not fully support the conclusions drawn by Varga et al (2010). Thus, additional experiments should be conducted in order to resolve this discrepancy. Firstly, in order to address the questions regarding the fornix injections, retrograde tracer injections should be deposited in this region. If this resulted in a similar pattern to what Varga et al (2010) reports, it would explain the discrepancy between the results in the two studies, and show where the calbindin population projects.

Furthermore, immunohistochemical studies with different chemical markers can address the questions regarding which marker(s) the commissurally projecting cell population are positive for. This knowledge can subsequently be used to develop transgenic animal models which have the potential to perform functional studies on the role of the commissural projection. More in detail, this would allow us to address questions regarding the function of the commissural projection in relation to the functionally defined cell types within MEC. More specifically, to test the hypothesis presented above, by “switching” off the commissural projection and see if this results in an accumulation of error and drift in the grid pattern over time.

Additionally, experiments should be done in order to explore the properties of the commissural projection along the entire dorsoventral axis of MEC. This study, in combination with immunohistochemical studies of the expression pattern of reelin and calbindin along the dorsoventral axis would address some of the questions concerning the dorsoventral axis of MEC raised in this thesis.

4.8. Conclusions

This thesis sheds light on the specificity of cell populations in superficial layers of MEC. The results indicate the presence of at least three separate cell populations with different projection targets and chemical profiles within superficial layers. Two separate cell populations are located within LII expressing different chemical markers. The cells projecting to DG are found throughout LII and express reelin, indicating that this protein can be used as a marker for this population in EC. As this protein was found to label parts of the commissural projection as well, it is however not a fully exclusive marker for the EC-DG population. The second population in LII resides deep within the layer at the border between LII and LIII and express the chemical marker calbindin. The projection pattern for this population still remains unknown. Lastly, the commissurally projecting cells reside mainly in a LIII of MEC and projects to contralateral MEC in a very specific and focal manner. The expression pattern for the majority of this population remains unknown, although parts of the projection were found to be positive for reelin. This separation of cell populations can have implications with regards to the already established functional cell populations within MEC.

5. REFERENCES

Adelmann, G., Deller, T. &Frotscher, M. 1996. Organization of identified fiber tracts in the rat fimbria-fornix: an anterograde tracing and electron microscopic study. *Anat Embryol,* 193**,** 481-493.

Amaral, D., Insausti, R. &Cowan, W. M. 1984. The commissural connections of the monkey hippocampal formation. *The Journal of Comparative Neurology,* 224**,** 307-336.

Amaral, D. &Lavenex, P. 2007. Hippocampal Neuroanatomy. *In:* Andersen, P., Morris, R., Amaral, D., Bliss, T. & O´Keefe, J. (eds.) *The Hippocampus Book.* Oxford: Oxford University Press.

Bentivoglio, M. &Swanson, L. W. 2001. On the fine structure of the pes Hippocampi major (with plates XIII-XXIII). *Brain Research Bulletin,* 54**,** 461-483.

Bonnevie, T., Dunn, B., Fyhn, M., Hafting, T., Derdikman, D., Kubie, J. L., Roudi, Y., Moser, E. I. &Moser, M.-B. 2013. Grid cells require excitatory drive from the hippocampus. *Nature Neuroscience*.

Borrell, V., Rio, J., Alcàntara, S., Derer, M., Martinez, A., D'Arcangelo, G., Nakajima, K., Derer, P., Curran, T. &Soriano, E. 1999. Reelin Regulates the Development and Synaptogenesis of the Layer-Specific Entorhino-Hippocampal Connections. *The journal of Neuroscience,* 19.

Brun, V. H., Leutgeb, S., Wu, H. Q., Schwarcz, R., Witter, M. P., Moser, E. I. &Moser, M. B. 2008a. Impaired spatial representation in CA1 after lesion of direct input from entorhinal cortex. *Neuron,* 57**,** 290-302.

Brun, V. H., Solstad, T., Kjelstrup, K. B., Fyhn, M., Witter, M. P., Moser, E. I. &Moser, M. B. 2008b. Progressive increase in grid scale from dorsal to ventral medial entorhinal cortex. *Hippocampus,* 18**,** 1200-12.

Burgalossi, A., Herfst, L., von Heimendahl, M., Förste, H., Haskic, K., Schmidt, M. &Brecht, M. 2011. Microcircuits of Functionally Identified Neurons in the Rat Medial Entorhinal Cortex. *Neuron,* 70**,** 773-786.

Burwell, R. 2001. Borders and cytoarchitecture of the perirhinal and postrhinal cortices in the rat. *Journal of Comparative Neurology,* 437**,** 17-41.

Burwell, R., Witter, M. P. &Amaral, D. G. 1995. Perirhinal and postrhinal corteces of the rat: A reveiw of the neuroanatomical literature and comparison with findings from the monkey brain. *Hippocampus,* 5**,** 390-408.

Canto, C. B. &Witter, M. P. 2011. Cellular properties of principal neurons in the rat entorhinal cortex. II. The medial entorhinal cortex. *Hippocampus*.

Canto, C. B., Wouterlood, F. G. &Witter, M. P. 2008. What Does the Anatomical Organization of the Entorhinal Cortex Tell Us? *Neural Plasticity,* 2008**,** 1-18.

Couey, J. J., Witoelar, A., Zhang, S.-J., Zheng, K., Ye, J., Dunn, B., Czajkowski, R., Moser, M.-B., Moser, E. I., Roudi, Y. &Witter, M. P. 2013. Recurrent inhibitory circuitry as a mechanism for grid formation. *Nature Neuroscience*.

Dailey, M., Marrs, G., Satz, J. &Waite, M. 1999. Exploring biological structure and function with confocal microscopy. *The Biological Bullitin,* 197.

Diana, M. A. &Marty, A. 2004. Endocannabinoid-mediated short-term synaptic plasticity: depolarization-induced suppression of inhibition (DSI) and depolarization-induced suppression of excitation (DSE). *British Journal of Pharmacology,* 142**,** 9-19.

Doeller, C. F., Barry, C. &Burgess, N. 2010. Evidence for grid cells in a human memory network. *Nature,* 463**,** 657-661.

Dolorfo, C., L. &Amaral, D. 1998. Entorhinal cortex of the rat, Topographic organization of the cells of origin of the perforant path projection to the dentate gyrus. *The Journal of Comparative Neurology,* 398**,** 25-48.

Domnisoru, C., Kinkhabwala, A. A. &Tank, D. W. 2013. Membrane potential dynamics of grid cells. *Nature,* 495**,** 199-204.

Eichenbaum, H., Yonelinas, A. R. &Ranganath, C. 2007. The Medial Temporal Lobe and Recognition Memory. *Annual Review of Neuroscience,* 30**,** 123-152.

Ekstrom, A., Kahana, M. J., Caplan, J. B., Fields, T. A., Isham, E. A., Newman, E. L. &Fried, I. 2003. Cellular networks underlying human spatial navigation. *Nature,* 425.

Esclapez, M., Tillakaratne, N., Kaufman, D., Tobin, A. &Houser, C. 1994. Comparative localization of two forms of glutaic acis decarboxylase and their mRNAs in rat brain supports the concept of functional differences between the forms. *The journal of Neuroscience,* 14.

Fujimaru, Y. &Kosaka, T. 1996. The distribution of two calcium binding proteins, calbindin D-28K and parvalbumin, in the entorhinal cortex of the adult mouse. *Neuroscience Research,* 24**,** 329-343.

Fyhn, M., Witter, M., Moser, E. I. &Moser, M.-B. 2004. Spatial Representation in the Entorhinal Cortex. *Science,* 305.

Gatome, C. W., Slomianka, L., Lipp, H. P. &Amrein, I. 2010. Number estimates of neuronal phenotypes in layer II of the medial entorhinal cortex of rat and mouse. *Neuroscience,* 170**,** 156-65.

Hafting, T., Fyhn, M., Molden, S., Moser, M.-B. &Moser, E. I. 2005. Microstructure of a spatial map in the entorhinal cortex. *Nature,* 436**,** 801-806.

Hamam, B., Kennedy, T., Alonso, A. &Amaral, D. 2000. Morphological and Electrophysiological Characteristics of Layer V Neurons of the Rat Medial Entorhinal Cortex. *The Journal of Comparative Neurology,* 418**,** 457-472.

Ino, T., Kaneko, T. &Mizuno, N. 2000. Intrinsic and commissural connections within the entorhinal cortex. An anterograde and retrograde tract-tracing study in the cat. *Neuroscience Research,* 36**,** 45-60.

Insausti, R., Herrero, m. T. &Witter, M. P. 1997. Entorhinal cortex of the rat: Cytoarchitectonic subdivisions and the origin and distribution of cortical efferents. *Hippocampus,* 7**,** 146-183.

Kerr, K. M., Agster, K. L., Furtak, S. C. &Burwell, R. D. 2007. Functional neuroanatomy of the parahippocampal region: The lateral and medial entorhinal areas. *Hippocampus,* 17**,** 697-708.

Killian, N. J., Jutras, M. J. &Buffalo, E. A. 2012. A map of visual space in the primate entorhinal cortex. *Nature,* 491**,** 761-4.

Kjoningsen, L., Leergaard, T., Witter, M. &Bjaalie, J. 2011. Digital atlas of anatomical subdivisions and boundaries of the rat hippocampal region. *Frontiers in Neuroscience,* 5.

Klink, R. &Alonso, A. 1997. Morphological Characteristics of Layer II Projection Neurons in the Rat Medial Entorhinal Cortex. *Hippocampus***,** 571-583.

Kloosterman, F., van Haeften, T., Witter, M. P. &Lopes da Silva, F. 2003. Electrophysiological characterization of interlaminar entorhinal connections: an essential link for re-entrance in the hippocampal-entorhinal system. *European Journal of Neuroscience,* 18**,** 3037-3052.

Kristensson, K. &Olsson, Y. 1971. Retrograde axonal transport of protein. *Brain Research,* 29**,** 363-365.

Krook-Magnuson, E., Varga, C., Lee, S.-H. &Soltesz, I. 2012. New dimensions of interneuronal specialization unmasked by principal cell heterogeneity. *Trends in Neurosciences,* 35**,** 175-184.

Köhler, C. 1986. Intrinsic connections of the retrohippocampal region in the rat brain. II. The medial entorhinal area. *Journal of Comparative Neurology,* 246**,** 149-169.

Köhler, C., Shipley, M., Srebro, B. &Harkmark, W. 1978. Some retrohippocampal afferents to the entorhinal cortex. Cells of origin as studied by HRP method in the rat and mouse. *Neuroscience Letters,* 10**,** 115-120.

Köhler, C., Wu, J.-Y. &Chan-Palay, V. 1985. Neurons and terminals in the retrohippocampal region in the rat's brain identidied by anti-γ-aminobutyric acid and anti-glutamic acid decarboxylase immunocytochemistry. *Anatomy and Embryology,* 173**,** 35-44.

Lanciego, J. L. &Wouterlood, F. G. 2011. A half century of experimental neuroanatomical tracing. *Journal of Chemical Neuroanatomy,* 42**,** 157-183.

Langston, R. F., Ainge, J. A., Couey, J. J., Canto, C. B., Bjerknes, T. L., Witter, M. P., Moser, E. I. &Moser, M. B. 2010. Development of the spatial representation system in the rat. *Science,* 328**,** 1576-80.

Lingenhöhl, K. &Finch, D. M. 1991. Morphological characterization of rat entorhinal neurons in vivo: soma-dendritic structure and axonal domains. *Experimental Brain Research,* 84**,** 57-74.

Miettinen, M., Koivisto, E., Riekkinen, P. &Miettinen, R. 1996. Coexistence of parvalbumin and GABA in nonpyramidal neurons of the rat entorhinal cortex. *Brain Research,* 706**,** 113-122.

Miettinen, M., Pitkänen, A. &Miettinen, R. 1997. Distribution of calretinin-immunoreactivity in the rat entorhinal cortex: coexistence with GABA. *Journal of Comparative Neurology,* 378**,** 363-378.

O´Keefe, J. 1976. Place Units in the Hippocampus of the Freely Moving Rat. *Experimental Neurology,* 51**,** 78-109.

O´Keefe, J. &Dostrovsky, J. 1971. The hippocampus as a spatial map. Preliminary evidence from unit activity in the freely-moving rat. *Brain Research,* 34.

Paxinos, G. &Watson, C. 2007. The Rat Brain in Stereotaxic Coordinates. London: Academic Press.

Pesold, C., Impagnatiello, F., Pisu, M. G., Uzdunov, D. P., Costa, E., Guidotti, A. &Caruncho, H. J. 1998. Reelin is preferentially expressed in neurons synthesizing gamma - aminobutyric acid in cortex and hippocampus of adult rats. *Proceedings of the National Academy of Sciences,* 95.

Ramos-Moreno, T., Galazo, M. J., Porrero, C., Martínez-Cerdeño, V. &Clascá, F. 2006. Extracellular matrix molecules and synaptic plasticity: immunomapping of intracellular and secreted Reelin in the adult rat brain. *European Journal of Neuroscience,* 23**,** 401-422.

Samu, D., Eros, P., Ujfalussy, B. &Kiss, T. 2009. Robust path integration in the entorhinal grid cell system with hippocampal feed-back. *Biological Cybernetics,* 101**,** 19-34.

Sargolini, F., Fyhn, M., Hafting, T., McNaughton, B. L., Witter, M. P., Moser, M. B. &Moser, E. I. 2006. Conjunctive representation of position, direction, and velocity in entorhinal cortex. *Science,* 312**,** 758-62.

Scoville, W. &Milner, B. 1957. Loss of recent memory after bilateral hippocampal lesions. *Journal of Neurology, Neurosurgery & Psychiatry,* 20.

Shaner, N. C., Steinbach, P. A. &Tsien, R. Y. 2005. A guide to choosing fluorescent proteins. *Nature Methods,* 2**,** 905-9.

Solstad, T., Boccara, C. N., Kropff, E., Moser, E. I. &Moser, M.-B. 2008. Representation of Geometric Borders in the Entorhinal Cortex. *Science,* 322**,** 1865-1868.

Solstad, T., Moser, E. I. &Einevoll, G. T. 2006. From grid cells to place cells: a mathematical model. *Hippocampus,* 16**,** 1026-31.

Soriano, E. &Del Rio, J. A. 2005. The cells of cajal-retzius: still a mystery one century after. *Neuron,* 46**,** 389-94.

Stensola, H., Stensola, T., Solstad, T., Frøland, K., Moser, M.-B. &Moser, E. I. 2012. The entorhinal grid map is discretized. *Nature,* 492**,** 72-78.

Steward, O. &Scoville, S. A. 1976. Cells of Origin of Entorhinal Cortical Afferents to the Hippocampus and Fascia Dentata of the Rat. *Journal of Comparative Neurology,* 169**,** 347-370.

Tamamaki, N. &Nojyo, Y. 1993. Projection of the entorhinal layer II neurons in the rat as revealed by intracellular pressure-injection of neurobiotin. *Hippocampus,* 3**,** 471-480.

Taube, J. S. 1998. Head direction cells and the neurophysiological basis for a sense of direction. *Progress in Neurobiology,* 55**,** 225-256.

Tolman, E. C. 1948. Cognitive Maps in Rats and Men *The Psychological Review,* 55**,** 189-208.

van Haeften, T., Baks-te-Bulte, L. n., Goede, P. H., Wouterlood, F. G. &Witter, M. P. 2003. Morphological and numerical analysis of synaptic interactions between neurons in deep and superficial layers of the entorhinal cortex of the rat. *Hippocampus,* 13**,** 943-952.

van Strien, N. M., Cappaert, N. L. M. &Witter, M. P. 2009. The anatomy of memory: an interactive overview of the parahippocampal–hippocampal network. *Nature Reviews Neuroscience,* 10**,** 272-282.

Varga, C., Lee, S. Y. &Soltesz, I. 2010. Target-selective GABAergic control of entorhinal cortex output. *Nature Neuroscience,* 13**,** 822-824.

Wills, T. J., Barry, C. &Cacucci, F. 2012. The abrupt development of adult-like grid cell firing in the medial entorhinal cortex. *Frontiers in Neural Circuits,* 6**,** 21.

Witter, M. 2007. The perforant path: projections from the entorhinal cortex to the dentate gyrus. 163**,** 43-61.

Witter, M., Griffioen, A. W., Jorritsma-Byham, B. &Krijnen, J. L. M. 1988. Entorhinal projections to the hippocampal CA1 region in the rat: an underestimated pathway. *Neuroscience Letters,* 85**,** 193-198.

Witter, M. &Wouterlood, F. G. 2002. *The Parahippocampal Region,* New York, Oxford University Press.

Witter, M. P. &Amaral, D. 1989. The three-dimensional organization of the hippocampal formation: a review of anatomical data. *Neuroscience* 31**,** 571-591.

Witter, M. P. &Amaral, D. 2004. Hippocampal Formation. *In:* Paxinos, G. (ed.) *The Rat Nervous System, Third Edition.* Elsevier Academic Press.

Witter, M. P. &Moser, E. I. 2006. Spatial representation and the architecture of the entorhinal cortex. *Trends in Neurosciences,* 29**,** 671-678.

Wouterlood, F. G. &Jasperse, B. 2001. Colocalization of calbindin D28k and GABA in the entorhinal cortex of the rat. *Abst.Soc.Neurosci,* 696.5.

Wouterlood, F. G. &Pothuizen, H. 2000. Sparse Colocalization of Somatostatin andGABA-Immunoreactivity in the Entorhinal Cortex of the Rat. *Hippocampus,* 10**,** 77-86.

Wouterlood, F. G., van Denderen, J. C. M., Van Haeften, T. &witter, M. P. 2000. Calretinin in the Entorhinal Cortex of the Rat, Distribution, Morphology, Ultrastructure of Neurons, and Co- localization With Gamma-Aminobutyric Acid and Parvalbumin. *The Journal of Comparative Neurology,* 425.

Yartsev, M. M., Witter, M. P. &Ulanovsky, N. 2011. Grid cells without theta oscillations in the entorhinal cortex of bats. *Nature,* 479**,** 103-7.

Zhang, S.-J., Ye, J., Miao, C., Tsao, A., Cerniauskas, I., Ledergerber, D., Moser, M. B. &Moser, E. I. 2013. Optpgenetic Dissection Of Entorhinal-Hippocampal Functional Connectivity. *Science,* 340.

APPENDIX I: NUMBER OF PLOTTED MARKERS IN EACH BRAIN

Brain 16957:

Total number of markers:

FB: 506

FG: 1065

FB + Reelin: 68

FG + Reelin: 804

FB + Calbindin: 2

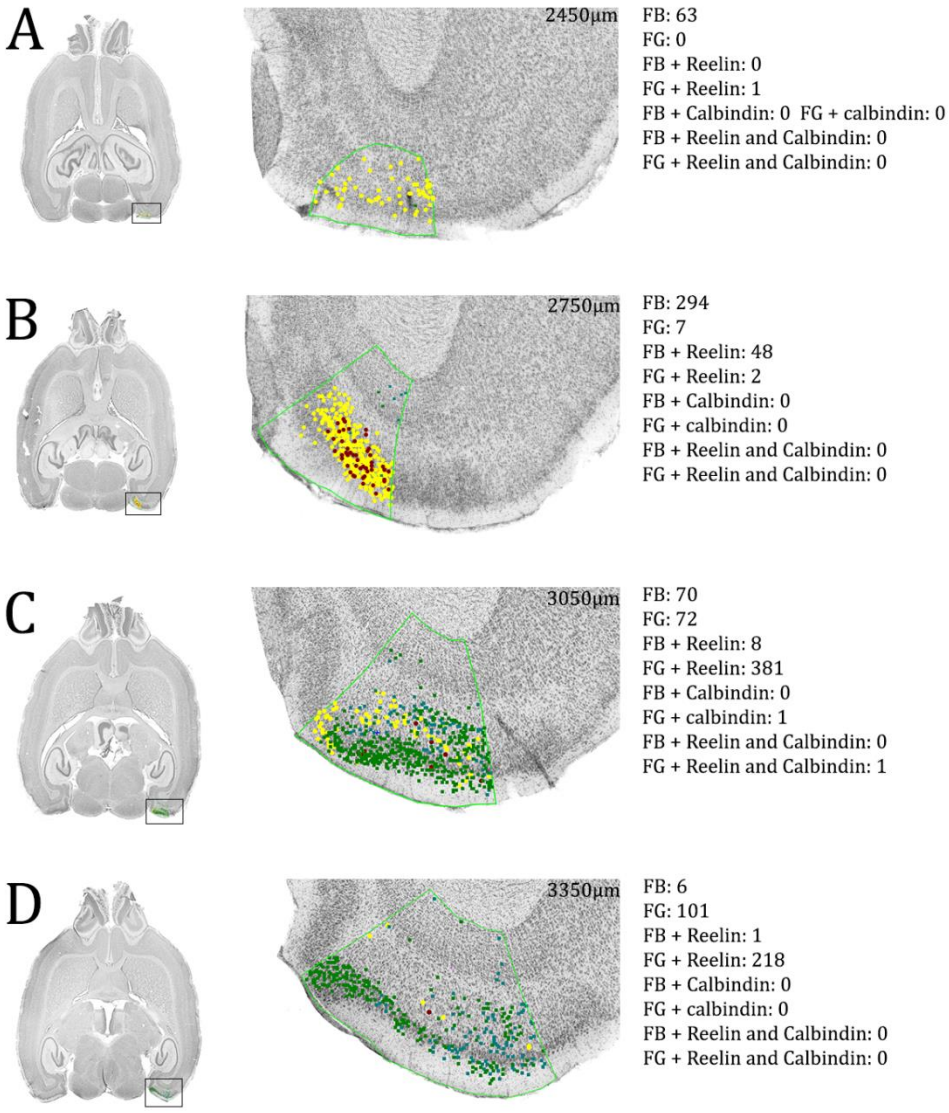

E

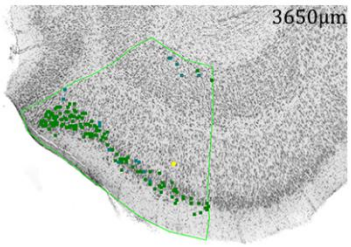

FB: 1
FG: 15
FB + Reelin: 0
FG + Reelin: 127
FB + Calbindin: 0
FG + calbindin: 0
FB + Reelin and Calbindin: 0
FG + Reelin and Calbindin: 0

F

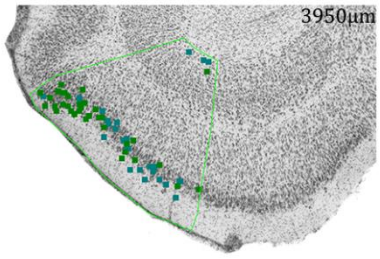

FB: 0
FG: 58
FB + Reelin: 0
FG + Reelin: 63
FB + Calbindin: 0
FG + calbindin: 0
FB + Reelin and Calbindin: 0
FG + Reelin and Calbindin: 0

G

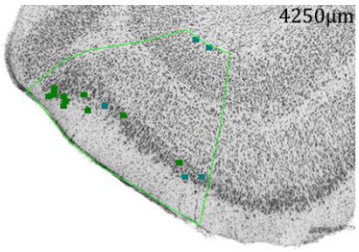

FB: 0
FG: 5
FB + Reelin: 0
FG + Reelin: 11
FB + Calbindin: 0
FG + calbindin: 0
FB + Reelin and Calbindin: 0
FG + Reelin and Calbindin: 0

H

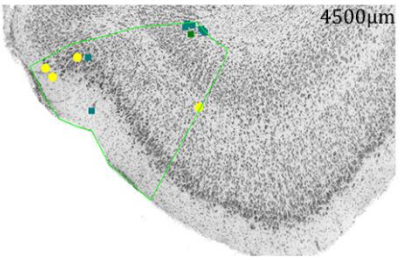

FB: 4
FG: 8
FB + Reelin: 0
FG + Reelin: 1
FB + Calbindin: 0
FG + calbindin: 0
FB + Reelin and Calbindin: 0
FG + Reelin and Calbindin: 0

BRAIN 16698 Calbindin:

Total number of markers:

FB: 446

FB + Reelin: 154

FB + Calbindin: 1

FB + Reelin + Calbindin: 1

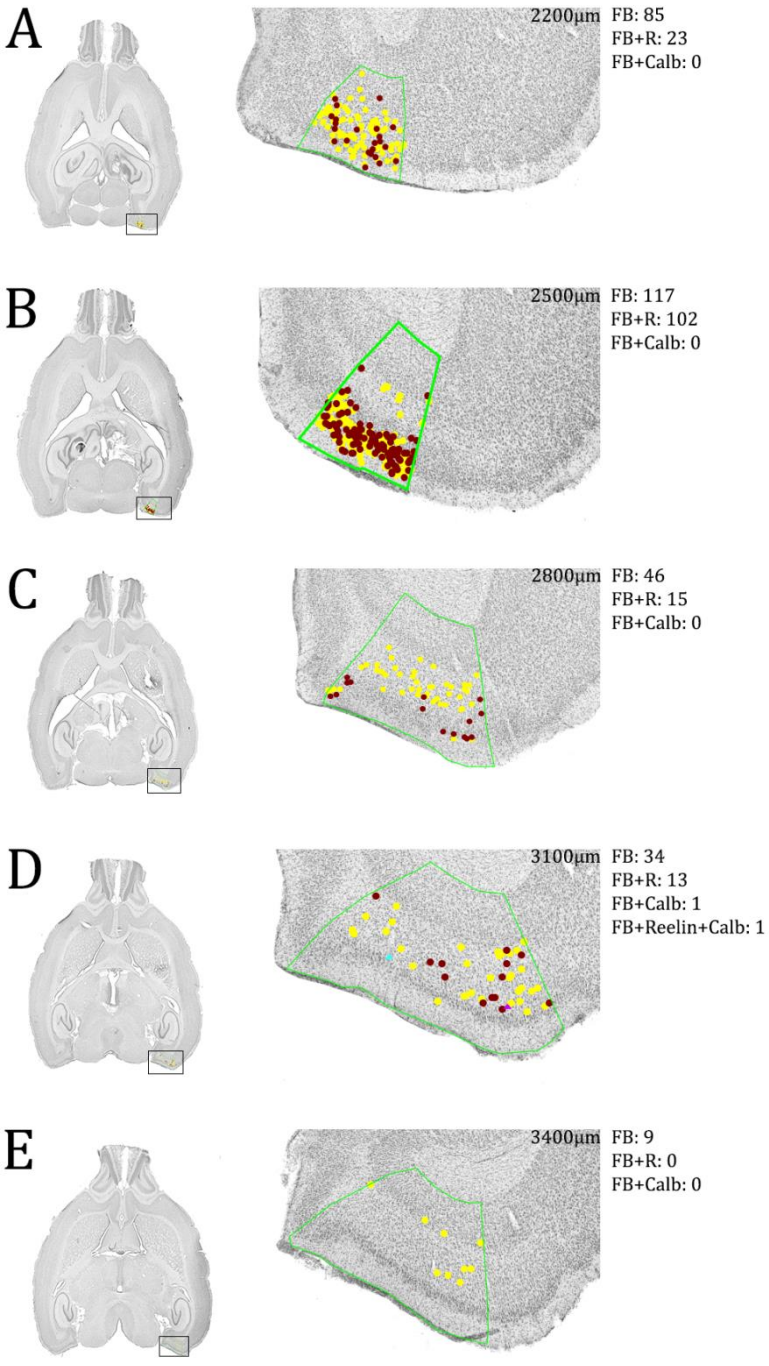

BRAIN 16698 Calretinin:

Total number of markers:

FB: 2202

FG: 522

Calretinin: 545

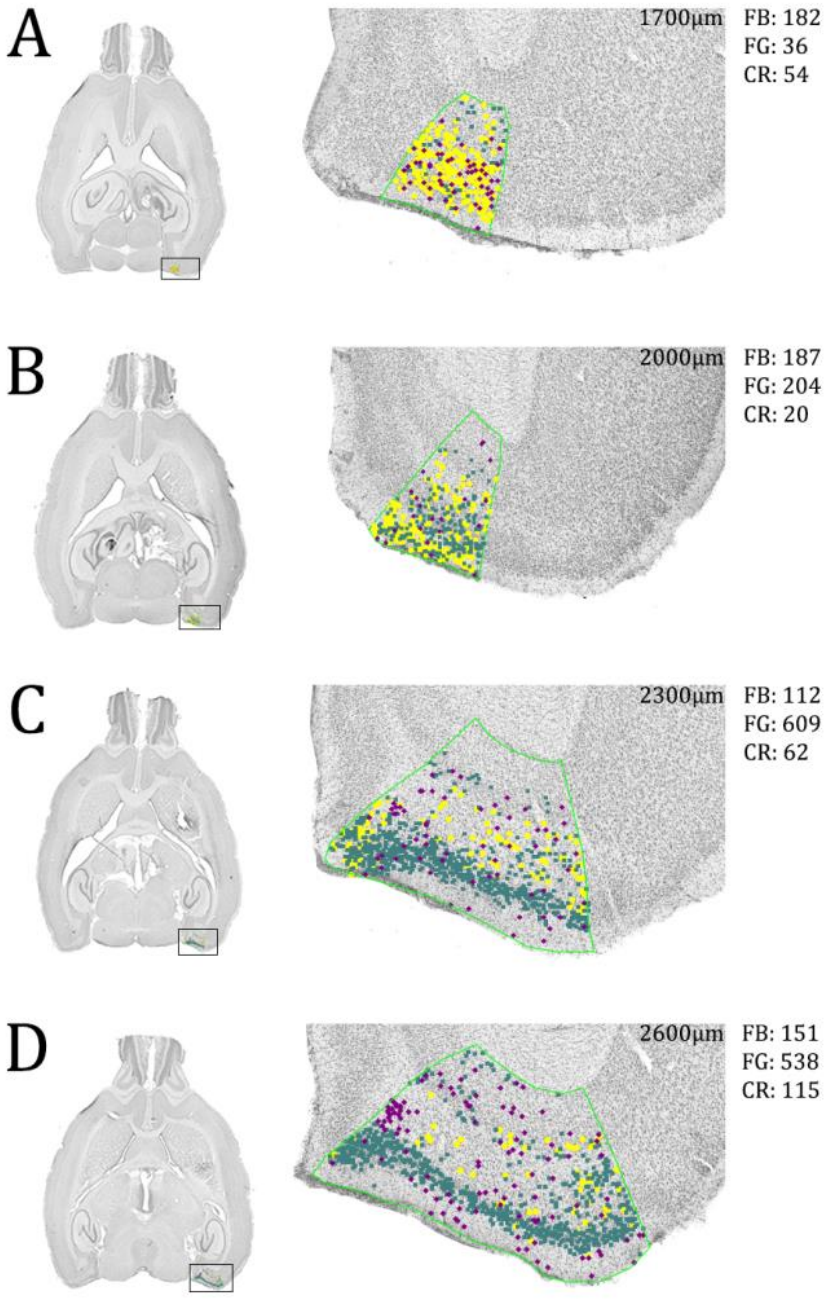

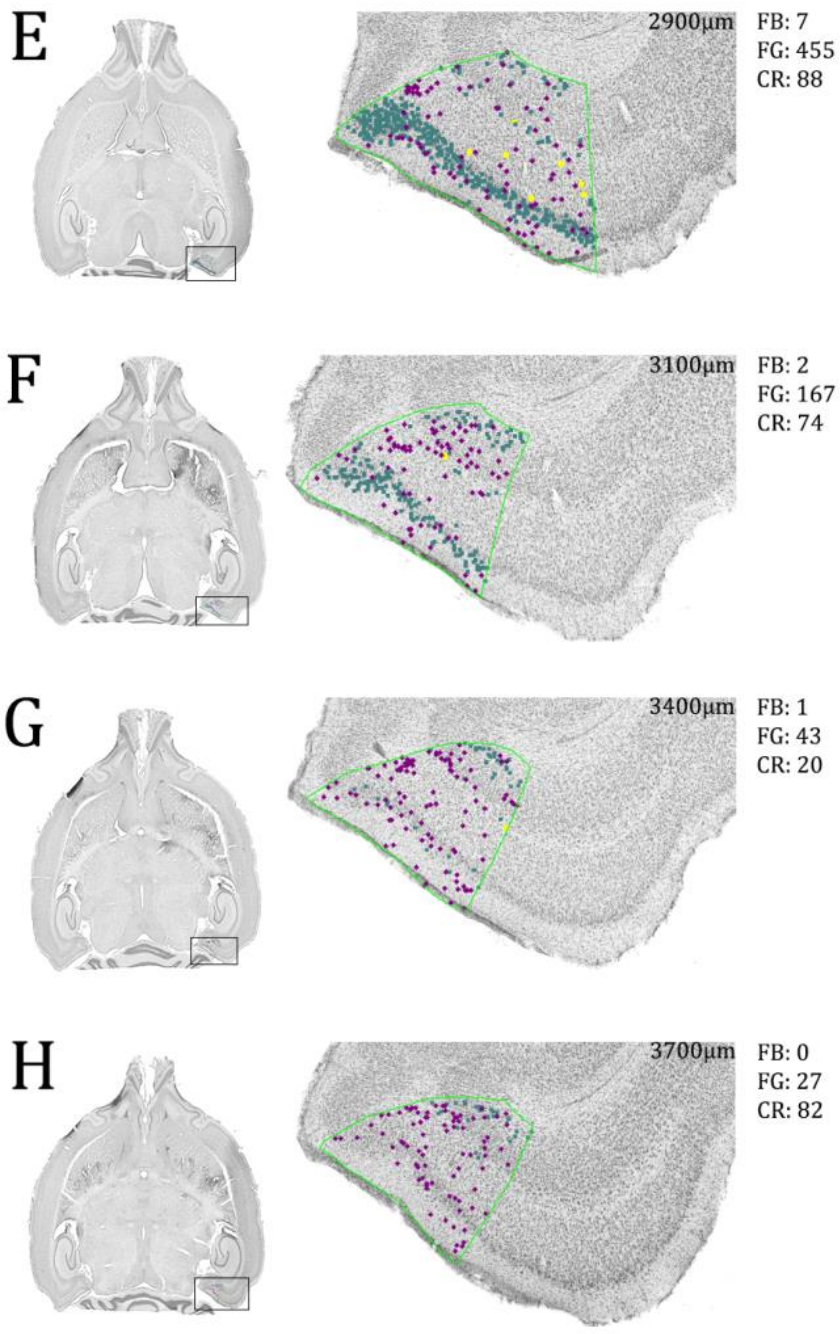
E
2900µm
FB: 7
FG: 455
CR: 88
F
3100µm
FB: 2
FG: 167
CR: 74
G
3400µm
FB: 1
FG: 43
CR: 20
H
3700µm
FB: 0
FG: 27
CR: 82

BRAIN 2413 eGFP-GAD67:

Total number of markers:

FB: 729

FG: 58

GFP: 530

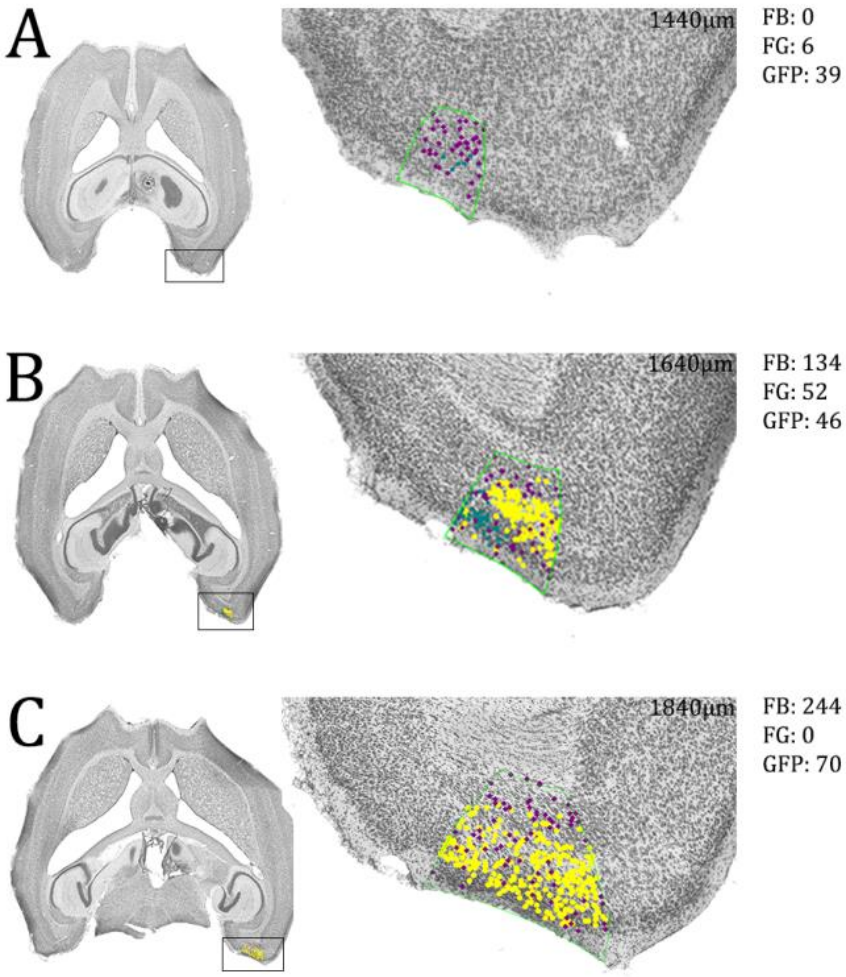

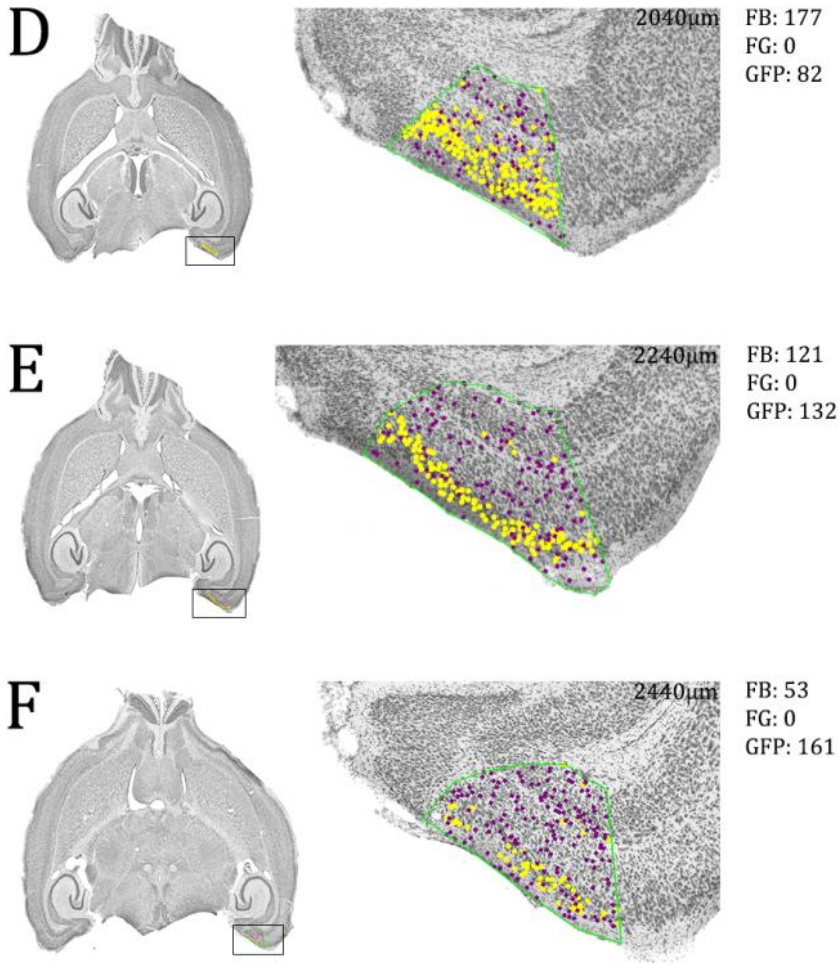
D
2040µm
FB: 177
FG: 0
GFP: 82
E
2240µm
FB: 121
FG: 0
GFP: 132
F
2440µm
FB: 53
FG: 0
GFP: 161

BRAIN 2628 eGFP-GAD67:

Total number of markers:

FB: 923

GFP: 748

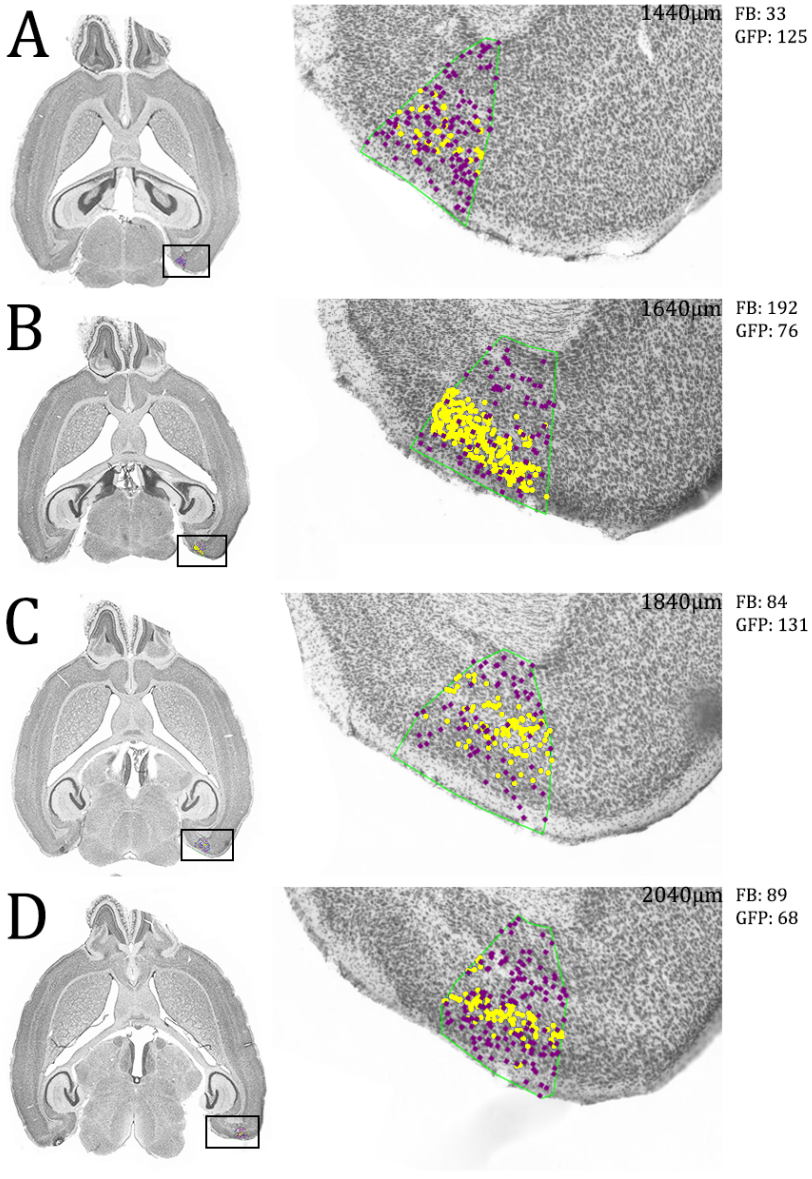

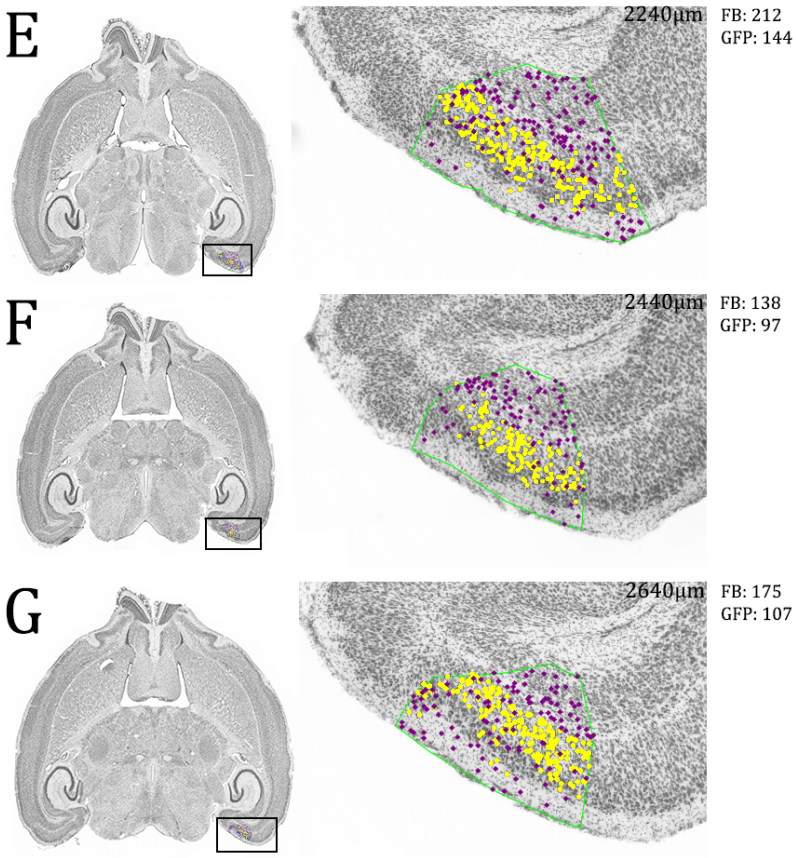
E
2240µm
FB: 212
GFP: 144
F
2440µm
FB: 138
GFP: 97
G
2640µm
FB: 175
GFP: 107

APPENDIX II: SURGERY PROTOCOL

Materials and equipment:

General:

- Surgery table
- Lights
- Stereomicroscope
- Vaporizer unit
- Induction box
- Stereotactic frame with injection tower (Kopf)
- Hair clippers
- Earbars
- Heating pad
- Drill
- Drill burr (0.9mm)
- Calculator

Surgical equipment:

- Instrument beaker with 70% ethanol
- Scalpel with # 6 blade
- Surgical scissors
- Tweezers
- Surgical drapes
- Hamilton needle (HamiltonCompany)
- Suture kit (Resorba)
- Cotten swabs
- Sugi (Kettenbach GmbH & co.)
- Iodine
- Sterile saline
- 70% ethanol
- Xylocane / Marcain
- Eye ointment (Novaris Healthcare AS)

- Syringes:

Three 1mL syringes with 25 gauge needles for Temgesic, Atropine and Marcain injections.

One 5mL syringe with 25 gauge needle for saline injections during the surgery to keep the animal hydrated.

One 10mL syringe with 18 gauge needle filled with saline. This is applied to the skull and surrounding skin to keep it hydrated during surgery.

- Tracers:

Fastblue: 2% diluted in 0.125M Phosphate buffer

Fluorogold: 2.5% diluted in H_2O

Surgical procedure:

- *For most surgeries the injection in MEC was performed first and the injection in DG second. It is however not necessary to do it in this order. Which hemisphere the two injections were made in alternated. This protocol describes the calculation of the MEC injection first.*
- *The Isoflurane level was progressively lowered down from 2.5% to 1% during the course of the surgery.*
- *Breathing was continuously monitored to ensure that the animal was fully anesthetized.*

Detailed surgery protocol:

- Prepare surgery room (Clean with alcohol, find all necessary equipment)
- Weigh the rat
- Prepare syringes with Temgesic, Atropine and Marcain based on the weight of the animal
- Anesthetize the animal in the induction box (Isoflurane at 4-4.5%)
- Shave the head of the animal
- Inject Temgesic and Atropine, wait 15-30 minutes
- Anesthetize the animal in the induction box (Isoflurane at 4-4.5%)
- Adjust Isoflurane % to 3 and transfer the rat to the heating pad.
- Place the nose of the rat in the mask
- Check responses to ensure that the animal is anesthetized (Toe pinching and eye blinking reflexes)
- Apply eye ointment
- Adjust ear bars, make sure the head is stable!
- Adjust Isoflurane down to 2.5%
- Disinfect the head with iodine and alcohol (3 times with each)
- Inject Marcain and wait a couple of minutes
- Make a straight midline incision with the scalpel
- Scrape off periost and visualize bregma and lambda
- Measure bregma and lambda height and adjust the head to a level position
- Drill a burr hole to visualize sagittal sinus, expand the hole if necessary in order to see clear edges
- Read out coordinates and calculate lateral coordinates
- Move to the appropriate lateral coordinate and to the interaural line
- Drill a burr hole to visualize the transverse sinus, expand the hole if necessary in order to see clear edges
- Calculate MEC coordinate from transverse sinus coordinate
- Drill burr hole at the calculated position
- Cut the dura with a dura knife and ensure that the needle can pass straight through

- Clean and check that the Hamilton needle is ok by testing it with saline
- Sonicate the vial with the tracer
- Load the needle with tracer
- Place the tracer filled needle in the tower
- Re-measure all coordinates
- Measure the height at the surface of the brain and calculate the depth of the injection
- Slowly lower the needle into position
- Wait 10 min
- Start the injection by injecting 50nl and wait a couple of minutes, this process is repeated until the correct amount have been injected (100-200nl)
- Wait 10 min after the injection is finished
- Slowly remove the needle
- Inject the animal with saline to keep it hydrated
- Move the needle back to the sagittal sinus
- Calculate the lateral coordinate for DG injection
- Move the appropriate lateral coordinate and to bregma
- Calculate the DG coordinate from the bregma position
- Drill a burr hole at the calculated position
- Cut the dura with a dura knife, ensure that the needle can pass straight through
- Clean and check that the Hamilton needle is ok by testing it with saline
- Sonicate the vial with the tracer
- Load the needle with tracer
- Place the tracer filled needle in the tower
- Re-measure all coordinates
- Measure the z direction and calculate the depth of the injection
- Slowly lower the needle into position
- Wait 10 min
- Start the injection by injecting 50nl and wait a couple of minutes, this process is repeated until the correct amount have been injected (100-200nl)
- Wait 10 min after the injection is finished
- Slowly remove the needle
- Clean the scull with saline and position the skin
- Suture the wound
- Clean the skull and suture area
- Inject the animal with saline to ensure that it is hydrated during the recovery
- Turn off Isoflurane and remove ear bars
- Place the animal in a heating cage to rest
- Administer Metacam orally when the animal is awake and responsive

- Return the animal to the home cage, make sure it has access to water and soft pellets
- Transfer the cage to the animal holding room

<u>Coordinates:</u>

Coordinates were adjusted continuously based on each previous injection to ensure the best possible hit. The coordinates listed below are representative for good injections in MEC and DG.

Dentate:

AP from bregma: -0.32mm

Medial - Lateral: 0.12 mm

Depth: 0.37mm

MEC:

AP from Sagittal sinus: 0.3mm

Medial - Lateral: 4.3mm

Depth 2.5mm

APPENDIX III: IMMUNOHISTOCHEMICTRY AND HISTOLOGY PROTOCOLS

Cresyl Violet:

- Dehydrate sections – 10 dips in each: 50-, 70-, 80-, 90-, 100-, 100-, and 100% ethanol
- Let sections sit 2 minutes in Xylene for clearing
- Rehydrate sections – 10 dips in each: 100-, 100-, 100-, 90-, 80-, 70-, and 50% ethanol
- Quick wash under running water
- Let sections sit in Cresyl Violet on shaker in dark (*time depends on the age of the solution*)
- Let sections sit in running water until all excess color is washed away
- Move sections into the Ethanol + Acetic Acid solution for a few seconds, while you gently shake the section holder
- Move sections quickly to a bath of cold water and let sections sit until all excess color is washed away
- Repeat point 7) and 8) until the sections are sufficiently light, while the contrast is still good
- Dehydrate sections – 10 dips in each: 50-, 70-, 80-, 90-, 100-, 100-, and 100% ethanol
- Move sections to Xylene baths for clearing (up to an hour).
- Coverslip sections

Solutions needed for Cresyl Violet protocol:

Ethanol

- 70%: mix 700 mL 96% ethanol (and 260mL distilled water.
- 80%: mix 500 mL 96% ethanol and 100mL distilled water.
- 90%: mix 800 mL 96% ethanol and 50 mL distilled water.

Ethanol + Acetic Acid

Mix 500 mL ethanol (70 %) and 2,5mL Acetic acid.

Cresyl violet

Dissolve 0.5 g Cresyl Violet in 500 mL distilled water. Leave in dark on stirrer with heat (about 60°C) for a couple of hours. Filtrate the solution into a non-transparent bottle. Store in dark at room temperature as light will make the solution crystallize.

Immunohistochemistry:

- Wash 3x15 min in PB (0.125M)
- 3x15 min in PB triton x (0.5%) (PBT)
- Blocking for 3 hours in PBT+ (PBT and normal goat serum 5%)
- Put primary antibodies in PBT+ and incubate in fridge for 24/48 hours (GFP: 24hours, Reelin and Calbindin: 48hours, Calretinin: 48/72hours)
- Wash 3x15 min in PB
- Secondary antibodies in PBT+ (concentration: 1:333) – Incubate for 2-3 hours at room temp, in the dark
- Wash 3x15 min in PB
- Mount and coverslip sections

Primary and secondary antibodies needed for immunohistochemistry protocols:

Calbindin (1:5000):

- *Primary: 30mL PBT+ and 6µl rabbit anti-Calbindin*
- *Secondary: 10mL PBT+ and 30µl goat anti-rabbit A546*

Reelin (1:1000):

- *Primary: 30mL PBT+ and 30µl mouse anti-Reelin*
- *Secondary: 10mL PBT+ and 30µl goat anti-mouse A488*

Calretinin (1:800):

- *Primary: 6.4mL PBT+ and 8µl mouse anti-Calretinin*
- *Secondary: 5mL PBT+ and 25µl goat anti-mouse A546*

General solutions needed for immunochemistry protocols:

Phosphate buffer (PB) 0.125M, pH 7.4:

Dilute 0.4M phosphate buffer

500 mL: 156 mL 0,4M phosphate buffer + 344 mL H_2O

0.5% Phosphate buffer Triton X:

500mL Phosphate buffer 0.125M + 2.5mL Triton-X-100

5% PBT+ (blocking agent):

50mL PBT + 2.5mL normal goat serum

APPENDIX IV: SOLUTIONS

Ringer (500mL):

0.85% NaCl (4.25g/500mL H2O)
0.025% KCl (0.125g/500mL H2O)
0.02% NaHCO3 (0.1g/500mL H2O)

Filtrate. Heat to about 40 °C before use, and set the pH to 6.9 using O2.

Make fresh ringer before every perfusion

10% Paraformaldehyde solution:

Heat 100 mL of H_2O to 60°C in the microwave oven. Measure 10 g of paraformaldehyde and add the water. Add a few drops of NaOH and leave the solution on a hot stirrer until the solution is clear.

4% Paraformaldehyde solution (500mL):

200 mL 10% paraformaldehyde
156 mL 0.4M phosphate buffer
144 mL H_2O

Set the pH to 7.4 using HCl and filtrate.

Make new fixative for every perfusion

Phosphate buffer (PB) 0.4M, pH 7.4:

A: NaH2PO4H2O 27.6 gram/500 mL H_2O
B: Na2HPO4H2O 35.6 gram/500 Ml H_2O

Make solutions A and B (start with B, it needs longer time). Add solution A to solution B until the pH is 7.4 (= 0.4M). Store in the dark in room temperature for up to one month.

Phosphate buffer (PB) 0.125M, pH 7.4:

Dilute 0,4M phosphate buffer. Store in refrigerator up to 1 week.

100 ml: 31.25 mL 0.4M phosphate buffer + 68.75 mL H_2O

500 ml: 156 mL 0.4M phosphate buffer + 344 mL H_2O

0.5% Phosphate buffer Triton X:

500mL Phosphate buffer 0.125M + 2.5mL Triton-X-100

5% PBT+ (blocking agent):

50mL PBT + 2.5mL normal goat serum (Abacam)

Gelatin:

Heat Tris-HCl to 60°C in the microwave oven. Add 0.2 gram gelatin per 100 mL Tris-HCl and put on stirrer until the gelatin has dissolved.

Store in refrigerator up to one week.

Sucrose solution:

Dissolve 30 g sucrose in 31.25 mL 0.4M phosphate buffer and 6.75 mL H_2O (or in 100 mL 0.125M phosphate buffer).

Cryoprotective solution (DMSO):

31.25 mL 0.4 M phosphate buffer

46.75 mL H_2O

20 mL glycerine

2 mL DMSO

APPENDIX V: LIST OF CHEMICALS AND ANTIBODIES

Antibodies and tracers:	**Manufacturer:**
Fastblue	EMS-grivory
Fluorogold	Fluorochrome
Goat anti-guinea pig A546	Invitrogen
Goat anti-mouse A488	Invitrogen
Goat anti-rabbit A546	Invitrogen
Mouse anti-Calretinin	Merck Millipore
Mouse anti-Reelin	Merck Millipore
Normal goat serum	Abacam
Rabbit anti-Calbindin	Merck Millipore
Rabbit anti-Calretinin	Merck Millipore
Rabbit anti-Green Fluorescent Protein	Life Technologies

Chemicals:	**Manufacturer:**
Cresyl Violet	Sigma-Aldrich
Dimethyl sulfoxide (DMSO)	VWR
Xylene	Merck
Entellan	Merck
Ethanol	Kemetyl Norge A/S
Gelatine	Oxoid
HCl	Merck
KCl	Merck
NaCl	VWR
NaHCO3	Merck
Paraformaldehyde	Merck
Phosphate buffer (PB)	Merck
Sucrose	VWR
Toluene	VWR
Tris (hydroxmethyl) aminomethane	Merck
Triton X-100	Merck